A subgrid model for nonlinear functions of a scalar

C. Pantano and S. Sarkar

Citation: Physics of Fluids (1994-present) **13**, 3803 (2001); doi: 10.1063/1.1410385
View online: http://dx.doi.org/10.1063/1.1410385
View Table of Contents: http://scitation.aip.org/content/aip/journal/pof2/13/12?ver=pdfcov
Published by the AIP Publishing

A subgrid model for nonlinear functions of a scalar

C. Pantano and S. Sarkar[a)]
Mechanical and Aerospace Engineering, University of California at San Diego, La Jolla, California 92093-0411

(Received 17 January 2001; accepted 22 August 2001)

In applications of large eddy simulation of turbulent flows, subgrid models are often required for closure of strongly nonlinear functions of a scalar. The Arrhenius dependence of the reaction rate on temperature, T, the T^4 dependence of radiation heat transfer, as well as the species mass fractions and temperature dependence on the mixture fraction in solutions of the strained laminar flamelet model are among some of the problems of interest. A moment-based reconstruction methodology is proposed here in which the scalar field is estimated by an approximate deconvolution operation but, unlike the usual deconvolution operation with given coefficients, the coefficients in the expansion are obtained by requiring that the statistical filtered moments of the scalar field up to a certain order are matched. The estimated scalar field is then used as a surrogate for the exact scalar field to directly calculate the subgrid contribution. Tests of the proposed approach are performed by using our direct numerical simulation database of scalar transport in a turbulent shear layer using two filter sizes: 12 points and 6 points per vorticity thickness. It is found that a simple moment-based model with one coefficient performs well for polynomial nonlinearities. The performance of the model in the case of an exponential Arrhenius-type nonlinearity is generally good and can be very good depending on the stoichiometric mixture fraction and the filter size. © *2001 American Institute of Physics.* [DOI: 10.1063/1.1410385]

I. INTRODUCTION

The theoretical modeling of combustion often involves strongly nonlinear functions of a scalar variable.[1] For example, the reaction rate exhibits an exponential dependence on the temperature; laminar flamelet theory[2] in nonpremixed combustion results in a nonlinear dependence of species mass fractions and temperature on a conserved scalar with the strain rate as a parameter; and, the energy loss rate for radiation heat transfer in the optically thin regime depends on the fourth power of the temperature. Filtering of such nonlinear terms in the governing equations that is performed as part of large eddy simulation (LES) approach to turbulent combustion results in subgrid contributions that must be modeled for closure of the LES approach. Thus, the common underlying problem is that, given a nonlinear function $f(Z)$ of a scalar Z, what is the subgrid contribution,

$$\overline{f(Z)}_{sg}=\overline{f(Z)}-f(\overline{Z}), \tag{1}$$

to its filtered value. In Eq. (1), filtering is represented by the overbar. Depending on the combustion model, the scalar in question may be a conserved scalar such as mixture fraction or a nonconserved scalar such as species mass fraction. We shall think of Z as being a mixture fraction, having a value of zero in the oxidizer feed stream and unity in the fuel feed stream.

In the present paper, we propose a model for the subgrid contribution, $\overline{f(Z)}_{sg}$, and evaluate its performance for the function Z^n, $n=2-8$, as well as the Arrhenius reaction rate nonlinearity $e^{-T_a/T}$, where the temperature is assumed to have a specified dependence, $T(Z)$, on the scalar and T_a, a specified constant, is the activation temperature. Direct numerical simulation (DNS) of passive scalar mixing in a turbulent shear layer is used for this *a priori* evaluation. It should be noted that the subgrid contribution in the case of $n=1$ is zero; therefore, interestingly, the assumption of infinitely fast chemistry that leads to piecewise linear dependence of the temperature and species on the mixture fraction also results in considerable simplification in LES away from the discontinuities in slope.

Approaches to modeling combustion in the LES context include the linear-eddy model[3] and methods based on probability density functions (PDF). In turbulent combustion applications[4,5] using the linear-eddy model, subgrid mixing is assumed to occur in lines following simple prescribed rules. The PDF approach has become popular in connection with modeling the subgrid contribution to scalar functions. In that approach, the so-called filtered PDF (also called subgrid PDF) is introduced to represent the stochastic variation of the scalar, Z, from its filtered value; a specific form is assumed for the subgrid PDF in the presumed PDF approach or, alternatively, a PDF transport equation is solved; and, thereby, the various filtered quantities that depend on the scalar are computed. The popular beta PDF which has been tested in previous studies[6,7] depends on two parameters, the filtered mean, $\overline{Z}$, and the filtered variance, $\overline{Z^2}$, and is employed to describe the statistical variation of the scalar value in a grid cell (more generally, the compact region associated with the filtering operation) around its expected value, $\overline{Z}$, in the presumed PDF approach. The filtered mean is explicitly avail-

a)Author to whom correspondence should be addressed. Electronic mail: ssarkar@ucsd.edu

able in an LES application while the filtered variance needs to be modeled. The scale similarity approach[7] with the coefficient calculated using an assumed scalar spectrum,[8] and a gradient model with the coefficient calculated with a dynamic procedure[9] have been used for obtaining the filtered variance. *A priori* tests of the beta PDF for subgrid scalar fluctuations for reactive scalars have been performed in previous studies using DNS data: Isotropic turbulence with infinitely fast chemistry[7] as well as with the strained laminar flamelet model;[10] in a nonpremixed shear layer with infinitely fast chemistry;[11] in a plane reacting jet using two-dimensional DNS;[12] and in a round reacting jet.[13] The latter two studies used a one-step, irreversible, finite-rate mechanism. An overall conclusion of the *a priori* tests is that the beta PDF model gives reasonable predictions of scalar moments if the *exact* subgrid scalar variance, obtained from the DNS, is used. Applications of the beta PDF model to performing LES of specific turbulent reacting flows are fewer, for example, the reacting jet simulation[14] that is based on the Lagrangian flamelet concept.

The model proposed here for the subgrid-scale (SGS) moments avoids the intermediate step of modeling the PDF of the subgrid-scale fluctuation and, as described in Sec. III, is based directly on known *physical-space* quantities. Furthermore, the scalar variance which is required in the PDF approach can also be obtained as a special case of the proposed model.

II. PRELIMINARIES

Consider a function $Z(\boldsymbol{x})$ represented on a discrete grid consisting of N points that spans a three-dimensional cubical domain of length $\mathcal{L}$. A Fourier transform pair is defined in the usual manner

$$\hat{Z}(\boldsymbol{\kappa}) = \frac{1}{(2\pi)^3}\int_{-\infty}^{\infty} e^{-i\boldsymbol{\kappa}\cdot\boldsymbol{x}} Z(\boldsymbol{x})\, d\boldsymbol{x}, \tag{2}$$

$$Z(\boldsymbol{x}) = \int_{-\infty}^{\infty} e^{i\boldsymbol{\kappa}\cdot\boldsymbol{x}} \hat{Z}(\boldsymbol{\kappa})\, d\boldsymbol{\kappa}, \tag{3}$$

where $\boldsymbol{\kappa}$ is the three-dimensional wave number and $\boldsymbol{x}$ is the spatial coordinate. In the present discussion only the top-hat filter is considered. Although the subsequent analysis can be extended to other kinds of filters, the compactness properties of the top-hat filter in physical space and its simplicity make it a good choice. Given a function $Z(\boldsymbol{x})$, the filtered field is obtained from

$$\overline{Z}(\boldsymbol{x}) = \frac{1}{\Delta_f^3}\int_{-\Delta_f/2}^{\Delta_f/2} Z(\boldsymbol{x}+\boldsymbol{r})\, d\boldsymbol{r}, \tag{4}$$

where Δ_f is the filter size and its transform in Fourier space is given by

$$\hat{\overline{Z}}(\boldsymbol{\kappa}) = \hat{G}(\boldsymbol{\kappa},\Delta_f)\hat{Z}(\boldsymbol{\kappa}), \tag{5}$$

where the transfer function is

$$\hat{G}(\boldsymbol{\kappa},\Delta_f) = \prod_{i=1}^{i=3} \frac{\sin(\kappa_i\Delta_f/2)}{(\kappa_i\Delta_f/2)}. \tag{6}$$

We define $\mathcal{F}(Z,m)$ as the linear operation of filtering the field, Z, successively m times, such that $\overline{Z}=\mathcal{F}(Z,1)$, $\bar{\bar{Z}}=\mathcal{F}(Z,2)$ and so on. The resolved grid spacing is $\Delta=\mathcal{L}/N$ and Δ_f/Δ is a parameter that determines the relative filter size. We note that, in an actual LES, the transfer function must be modified from Eq. (6) to account for the filtering implicit in the numerical method and grid resolution. The consequences of such a modification are discussed in the Appendix. However, for the formal development of the proposed model, it is sufficient to consider the filter transfer function, $\hat{G}$.

A. Nonlinear function

Given an arbitrary nonlinear function $f(Z)$, it is possible to perform a Taylor series expansion around a point Z_0, such that

$$f(Z) = f(Z_0) + f'(Z_0)(Z-Z_0) + \frac{f''(Z_0)}{2}(Z-Z_0)^2 + \cdots. \tag{7}$$

Filtering Eq. (7) and substituting $Z_0=\overline{Z}$ gives

$$\overline{f(Z)} - f(\overline{Z}) = \frac{f''(\overline{Z})}{2}(\overline{Z^2}-\overline{Z}^2) + \cdots. \tag{8}$$

It is clear that if a good procedure to calculate lower-order nonlinearities, for example, $\overline{Z^2}$, is available then it may be possible to obtain a good representation of the left-hand-side (l.h.s.) of Eq. (8). The objective then is to obtain a SGS model in which the parameters are chosen appropriately so as to obtain a good representation of lower-order nonlinearities. We begin by studying how the average contribution of $\overline{Z^2}$ might be obtained.

B. Reconstruction

It is possible to reconstruct some properties of the original field from its filtered values given the explicit form of the filter. The approximate deconvolution method,[15] and the inverse modeling method[16] are two examples. If we represent G as the nonzero filtering operator, then, following,[15] in operational form

$$Z = \frac{1}{G}\overline{Z} = \frac{1}{1-(1-G)}\overline{Z}$$

$$= \overline{Z} + (\overline{Z}-\bar{\bar{Z}}) + (\overline{Z}-2\bar{\bar{Z}}+\overline{\bar{\bar{Z}}}) + \cdots. \tag{9}$$

This procedure is correctly posed only if G is nonzero, and Eq. (9) does not apply to wave numbers where $G=0$. The inverse filtering operation cannot reconstruct all the high wave number information that has been removed by the filtering operation but provides one possible ''approximation'' of the exact field useful for obtaining required subgrid models. Previous studies[15,16] have shown that such a reconstruction procedure works well for the subgrid Reynolds stress. Let Z^* be a truncation of the series in the right-hand-side (r.h.s.) of Eq. (9). Once Z^* is calculated, the nonlinear function $f(Z)$ is approximated by $f(Z^*)$. Any further operation is performed using $f(Z^*)$ instead of $f(Z)$.

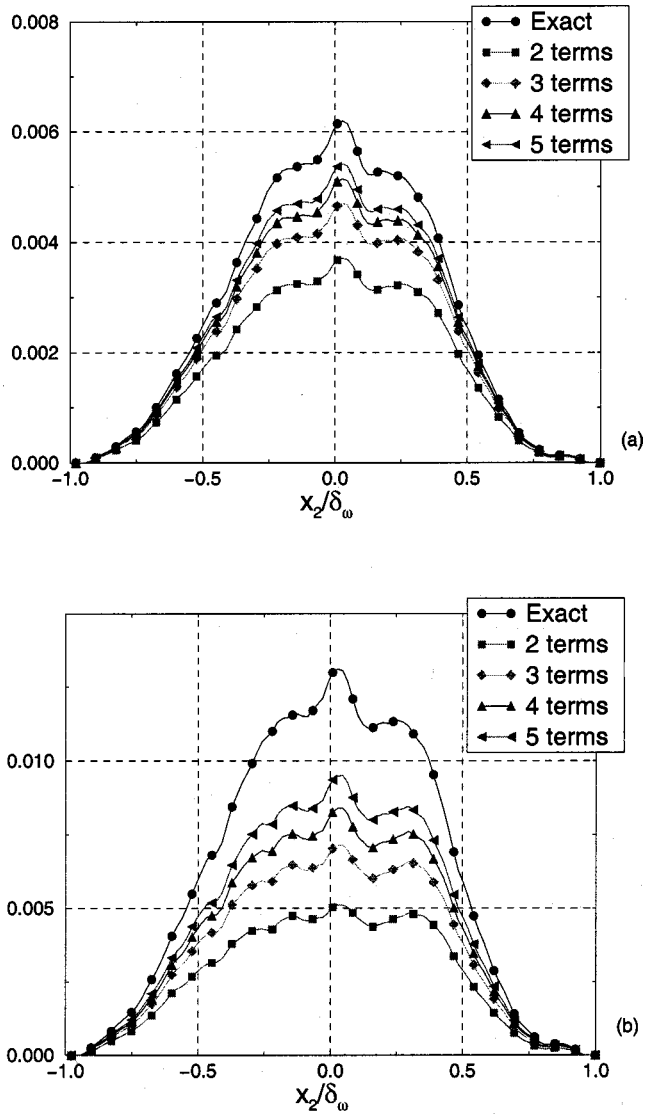

FIG. 1. Profiles of the subgrid scalar variance, $\langle \overline{Z^2_{sg}} \rangle$; (a) $\Delta_f/\Delta=4$, (b) $\Delta_f/\Delta=8$. Results with truncations of different order in the approximate deconvolution method are compared with the exact profile.

A priori tests have been performed using our DNS database of the temporal mixing layer to study the behavior of this approximate deconvolution procedure. The DNS database is described in Sec. VI. The temporal mixing layer is homogeneous in the x_1 and x_3 directions and the statistics (denoted by $\langle \cdot \rangle$ and obtained by x_1-x_3 plane averages) vary in the x_2 direction. Profiles of the expected value, $\langle \overline{Z^2}_{sg} \rangle$, of the subgrid contribution to $\overline{Z^2}$, as a function of the cross-stream coordinate normalized by the vorticity thickness, δ_ω, are shown in Fig. 1. The effect of increasing the number of terms in the expansion, Eq. (9), is shown for the filter widths $\Delta_f/\Delta=4$ and 8. As can be seen, even with five terms, requiring the calculation of $\mathcal{F}(Z,5)$, we can only recover 88% of the peak contribution in the first case and 73% in the case with $\Delta_f/\Delta=8$. Although the tendency is in the right direction, the number of terms required, even for a simple nonlinear function such as Z^2, becomes prohibitive. Therefore, we introduce an alternative approach as described below.

III. PROPOSED APPROACH TO SGS MODELING

The proposed modeling approach consists of assuming a functional form for the dependence of the estimated scalar, Z_M, on the multiple filtered fields, $\mathcal{F}(Z,m)$. This estimated scalar is then used as a surrogate for the exact scalar field in the calculation of $\overline{f(Z)}$, so that the model for the required subgrid contribution becomes

$$\overline{f(Z)}-f(\overline{Z})=\overline{f(Z_M)}-f(\overline{Z}_M). \tag{10}$$

Equation (10) satisfies the following consistency properties. First, for a linear function, $f(Z)=aZ+b$, Eq. (10) is exact for any approximation Z_M to the exact scalar field Z. Second, the proposed model, the r.h.s. of Eq. (10), transforms in the same way as the l.h.s. under a linear mapping of the scalar. For example, the exact subgrid variance is invariant under a translation, i.e.; change of the reference value by Z_0,

$$\overline{f(Z+Z_0)_{sg}}=\overline{(Z+Z_0)^2}-(\overline{Z}+Z_0)^2=\overline{f(Z)_{sg}}. \tag{11}$$

The approximation proposed here for Z_M, see Eq. (52), transforms to Z_M+Z_0 under a translation, obeying the same transformation rule as the exact scalar field, Z. It then follows that the subgrid variance calculated using the surrogate scalar, Z_M, is also invariant under a translation. The subgrid contribution for Z^2 is very important because it is the leading order term in a Taylor series expansion of an arbitrary function as shown by Eq. (8). During the course of this study, it was found that an alternative model, $\overline{f(Z)}=\overline{f(Z_M)}$, which did not satisfy the aforementioned invariance property of the subgrid variance leads to a deterioration in the pointwise behavior.

The estimated scalar field, Z_M, depends on unknown coefficients that must be determined. In order to obtain these unknown coefficients, a set of constraints is imposed on the model. Finally, the set of equations is solved by any means available; in the present case, by assuming a theoretical turbulence spectrum that permits closure of the constraint equations.

Consider a model, M, that depends on the filtered fields $\{\overline{Z},\bar{\bar{Z}}, \ldots,\mathcal{F}(Z,m)\}$, namely

$$Z_M(\mathbf{x})=M(\{c_0,c_1,\ldots,c_n\},\{\overline{Z},\bar{\bar{Z}}, \ldots,\mathcal{F}(Z,m)\}). \tag{12}$$

The model coefficients, $\{c_0,c_1,\ldots,c_n\}$, are chosen in such a way that a predefined cost function is optimal. Each cost function generates a family of model parameters that, in principle, depends on filter size and the local conditions of the flow. A member of the family of models, Eq. (12), is an extension of the deconvolution procedure[15]

$$Z_M=\overline{Z}+c_0(\overline{Z}-\bar{\bar{Z}})+c_1(\overline{Z}-2\bar{\bar{Z}}+\bar{\bar{\bar{Z}}})+\cdots, \tag{13}$$

where the coefficients, $\{c_0,c_1,\ldots,c_n\}$, are allowed to vary instead of being fixed to be unity. In the present work we will consider only this model due to its simplicity. Its transfer function is

$$\frac{\hat{Z}_M}{\hat{Z}}=\hat{M}(c_l,\hat{G},\hat{G}^2,\ldots), \tag{14}$$

where the hat denotes the Fourier transform.

IV. MOMENT-BASED SUBGRID MODELING

In order to obtain a set of equations that permits the calculation of the coefficients c_l, conditions or constraints have to be chosen. Among the multiple choices that can be made, the simplest one is to make the statistical mean filtered moments that appear in the Taylor series expansions of the modeled field equal to the corresponding filtered moments of the exact field. This condition is expressed in mathematical form by

$$\begin{aligned}
&\int_\Omega \overline{Z^2}-\overline{Z}^2 d\boldsymbol{x}=\int_\Omega \overline{Z_M^2}-\overline{Z}_M^2 d\boldsymbol{x},\\
&\int_\Omega \overline{Z^3}-\overline{Z}^3 d\boldsymbol{x}=\int_\Omega \overline{Z_M^3}-\overline{Z}_M^3 d\boldsymbol{x},\\
&\cdots=\cdots,\\
&\int_\Omega \overline{Z^n}-\overline{Z}^n d\boldsymbol{x}=\int_\Omega \overline{Z_M^n}-\overline{Z}_M^n d\boldsymbol{x},
\end{aligned} \tag{15}$$

where Ω is the appropriate domain for calculating the average. The required number of equations of this form is chosen equal to the number of unknown coefficients. Another possibility is to consider a cost function of the form

$$I(c_l)=\int_\Omega ((\overline{Z^2}-\overline{Z}^2)-(\overline{Z_M^2}-\overline{Z}_M^2))^2 d\boldsymbol{x}, \tag{16}$$

from which the values of the coefficients are calculated by a standard minimization procedure. In a more complex model, a combination of both methods can be used.

A. One-parameter model

Consider now the simple one-parameter model

$$Z_M=\overline{Z}+c_0(\overline{Z}-\widetilde{Z}), \tag{17}$$

where the tilde represents a test filter with cut-off wave number, κ_t, that, in general could be different from the principal filter cutoff wavenumber κ_f. As discussed in the Appendix, there are situations where a test filter, different from the main filter, may be useful. The Appendix discusses the model performance when the test and main filters are not identical. Henceforth, in the main body of the paper, we will assume that the test filter is the same as the main filter so that the model becomes

$$Z_M=\overline{Z}+c_0(\overline{Z}-\bar{\bar{Z}}), \tag{18}$$

whose transfer function is

$$\hat{M}_1=\hat{G}(1+c_0(1-\hat{G})). \tag{19}$$

The equation for c_0 is obtained by requiring that the exact and model fields have averaged filtered moments of order 2 that are equal

$$\int_\Omega \overline{Z^2}-\overline{Z}^2 d\boldsymbol{x}=\int_\Omega \overline{Z_M^2}-\overline{Z}_M^2 d\boldsymbol{x}. \tag{20}$$

Defining $\phi(\boldsymbol{x})=\overline{Z^2}(\boldsymbol{x})$ and $\phi_M(\boldsymbol{x})=\overline{Z_M^2}(\boldsymbol{x})$, and using the inverse Fourier transform formula

$$\phi(\boldsymbol{x})=\int_{-\infty}^{\infty} e^{i\boldsymbol{k}\cdot\boldsymbol{x}}\hat{\phi}(\boldsymbol{k})d\boldsymbol{k}, \tag{21}$$

where $\hat{\phi}(\boldsymbol{k})$ is the Fourier transform of $\phi(\boldsymbol{x})$, it is possible to write the first term on the l.h.s. in Eq. (20) as

$$\int_\Omega \overline{Z^2}d\boldsymbol{x}=\int_\Omega \phi(\boldsymbol{x})d\boldsymbol{x}=\int_\Omega\int_{-\infty}^{\infty} e^{i\boldsymbol{k}\cdot\boldsymbol{x}}\hat{\phi}(\boldsymbol{k})d\boldsymbol{k}d\boldsymbol{x}. \tag{22}$$

Exchanging integrals and taking into account the relation

$$\delta(\boldsymbol{k})=\frac{1}{(2\pi)^3}\int_{-\infty}^{\infty} e^{i\boldsymbol{k}\cdot\boldsymbol{x}}d\boldsymbol{x}, \tag{23}$$

for a three-dimensional space, Ω, it follows that

$$\int_\Omega \overline{Z^2}d\boldsymbol{x}=(2\pi)^3\hat{\phi}(0). \tag{24}$$

The same simplification is applied to the first term in the r.h.s. of Eq. (20). Defining $\psi(\boldsymbol{x})=\overline{Z^2}(\boldsymbol{x})$ and $\psi_M(\boldsymbol{x})=\overline{Z_M^2}(\boldsymbol{x})$ and applying the same procedure to the second term in the l.h.s. and r.h.s. of Eq. (20), we get the equivalent of Eq. (20) in spectral space

$$\hat{\phi}(0)-\hat{\psi}(0)=\hat{\phi}_M(0)-\hat{\psi}_M(0). \tag{25}$$

The Fourier transform of $\phi(\boldsymbol{x})=\overline{Z^2}(\boldsymbol{x})$ can be expressed as a function of that of $Z(\boldsymbol{x})$ using Parseval's convolution integrals

$$\hat{\phi}(\boldsymbol{k})=\hat{G}(\boldsymbol{k})\int_{-\infty}^{\infty}\hat{Z}(\boldsymbol{\kappa}_0)\hat{Z}(\boldsymbol{\kappa}-\boldsymbol{\kappa}_0)d\boldsymbol{\kappa}_0. \tag{26}$$

Setting $\boldsymbol{\kappa}=0$ and taking into account that $\hat{Z}(-\boldsymbol{\kappa}_0)=\hat{Z}^*(\boldsymbol{\kappa}_0)$ and $\hat{G}(0)=1$ gives $\hat{\phi}(0)$, and a similar procedure gives $\hat{\phi}_M(0)$. The resulting expressions are

$$\hat{\phi}(0)=\int_{-\infty}^{\infty}\hat{Z}(\boldsymbol{\kappa}_0)\hat{Z}^*(\boldsymbol{\kappa}_0)d\boldsymbol{\kappa}_0, \tag{27}$$

$$\hat{\phi}_M(0)=\int_{-\infty}^{-\infty}\hat{Z}_M(\boldsymbol{\kappa}_0)\hat{Z}_M^*(\boldsymbol{\kappa}_0)d\boldsymbol{\kappa}_0. \tag{28}$$

The Fourier transform of $\psi(\boldsymbol{x})=\overline{Z^2}(\boldsymbol{x})$ can also be expressed as a function of that of $Z(\boldsymbol{x})$ using Parseval's convolution integrals

$$\hat{\psi}(\boldsymbol{\kappa})=\int_{-\infty}^{\infty}\hat{G}(\boldsymbol{\kappa}_0)\hat{Z}(\boldsymbol{\kappa}_0)\hat{G}(\boldsymbol{\kappa}-\boldsymbol{\kappa}_0)\hat{Z}(\boldsymbol{\kappa}-\boldsymbol{\kappa}_0)d\boldsymbol{\kappa}_0, \tag{29}$$

and setting again $\boldsymbol{\kappa}=0$ and taking into account that $\hat{Z}(-\boldsymbol{\kappa}_0)=\hat{Z}^*(\boldsymbol{\kappa}_0)$ gives $\hat{\psi}(0)$, and a similar procedure gives $\hat{\psi}_M(0)$. The resulting expressions are

$$\hat{\psi}(0)=\int_{-\infty}^{\infty}\hat{G}(\boldsymbol{k}_0)\hat{G}^*(\boldsymbol{k}_0)\hat{Z}(\boldsymbol{\kappa}_0)\hat{Z}^*(\boldsymbol{\kappa}_0)d\boldsymbol{\kappa}_0, \tag{30}$$

$$\hat{\psi}_M(0)=\int_{-\infty}^{\infty}\hat{G}(\boldsymbol{k}_0)\hat{G}^*(\boldsymbol{k}_0)\hat{Z}_M(\boldsymbol{\kappa}_0)\hat{Z}_M^*(\boldsymbol{\kappa}_0)d\boldsymbol{\kappa}_0. \tag{31}$$

Introducing $\hat{Z}_M(\boldsymbol{\kappa})=\hat{Z}(\boldsymbol{\kappa})\hat{M}_1(c_0,\boldsymbol{\kappa})$, where $\hat{M}_1$ is defined by Eq. (19), the following form of Eq. (25) is obtained:

$$\int_{-\infty}^{\infty} \hat{Z}(\boldsymbol{\kappa}_0)\hat{Z}^*(\boldsymbol{\kappa}_0)[1-\hat{M}_1(c_0,\boldsymbol{\kappa}_0)\hat{M}_1^*(c_0,\boldsymbol{\kappa}_0)] \times[1-\hat{G}(\boldsymbol{k}_0)\hat{G}^*(\boldsymbol{k}_0)]d\boldsymbol{\kappa}_0=0. \quad (32)$$

Substituting the expression, Eq. (19), for $\hat{M}_1(c_0,\boldsymbol{\kappa}_0)$, we get

$$0=a_0+c_0a_1+c_0^2a_2, \quad (33)$$

where

$$a_0=\int_{-\infty}^{\infty} E_Z(\boldsymbol{\kappa}_0)[\hat{G}(\boldsymbol{\kappa}_0)\hat{G}^*(\boldsymbol{\kappa}_0)-1] \times[1-\hat{G}(\boldsymbol{k}_0)\hat{G}^*(\boldsymbol{k}_0)]d\boldsymbol{\kappa}_0, \quad (34)$$

$$a_1=\int_{-\infty}^{\infty} E_Z(\boldsymbol{\kappa}_0)\hat{G}(\boldsymbol{\kappa}_0)\hat{G}^*(\boldsymbol{\kappa}_0)[2-\hat{G}(\boldsymbol{\kappa}_0)-\hat{G}^*(\boldsymbol{\kappa}_0)] \times[1-\hat{G}(\boldsymbol{k}_0)\hat{G}^*(\boldsymbol{k}_0)]d\boldsymbol{\kappa}_0, \quad (35)$$

$$a_2=\int_{-\infty}^{\infty} E_Z(\boldsymbol{\kappa}_0)\hat{G}(\boldsymbol{\kappa}_0)\hat{G}^*(\boldsymbol{\kappa}_0)[1-\hat{G}(\boldsymbol{\kappa}_0)] \times[1-\hat{G}^*(\boldsymbol{\kappa}_0)][1-\hat{G}(\boldsymbol{k}_0)\hat{G}^*(\boldsymbol{k}_0)]d\boldsymbol{k}_0, \quad (36)$$

with $E_Z(\boldsymbol{\kappa})=\hat{Z}(\boldsymbol{\kappa})\hat{Z}^*(\boldsymbol{\kappa})$. If the spectrum of the scalar and the characteristics of the filter are known, it is possible to solve the quadratic, Eq. (33), for c_0. Thus, the coefficient depends on both the filter characteristics and, through the scalar spectrum, on the state of the turbulent field. This coefficient can be tabulated *a priori* for a given filter making the calculation in a LES code straightforward, provided that a good approximation of the scalar spectrum is known. The low wave number part of the spectrum where $E_Z(\boldsymbol{\kappa})$ increases with increasing k is problem-dependent and difficult to model. However, the contribution of the low wave number part of the spectrum to Eqs. (34)–(36) is negligible since $\hat{G}(\boldsymbol{\kappa})\to 1$ for $\boldsymbol{\kappa}\to 0$. Therefore, the proposed model does not depend on the spectral shape at the low wave number end. The influence of the assumed shape of the model spectrum in other wave number ranges is discussed in more detail in the following section.

B. Calculation of c_0

In *a priori* tests, the direct approach is to use the DNS database in order to calculate the required integrals, Eq. (20), from where c_0 can be calculated. This approach is reduced to solving the following equation for c_0, where the integrals are calculated from the DNS database:

$$\int_\Omega \overline{Z^2}-\overline{Z}^2 d\boldsymbol{x}=\int_\Omega \overline{\overline{Z}^2}-\bar{\bar{Z}}^2 d\boldsymbol{x} +2c_0\int_\Omega \overline{\overline{Z}(\overline{Z}-\bar{\bar{Z}})}-\bar{\bar{Z}}(\bar{\bar{Z}}-\bar{\bar{\overline{Z}}})d\boldsymbol{x} +c_0^2\int_\Omega \overline{(\overline{Z}-\bar{\bar{Z}})^2}-(\bar{\bar{Z}}-\bar{\bar{\overline{Z}}})^2 d\boldsymbol{x}, \quad (37)$$

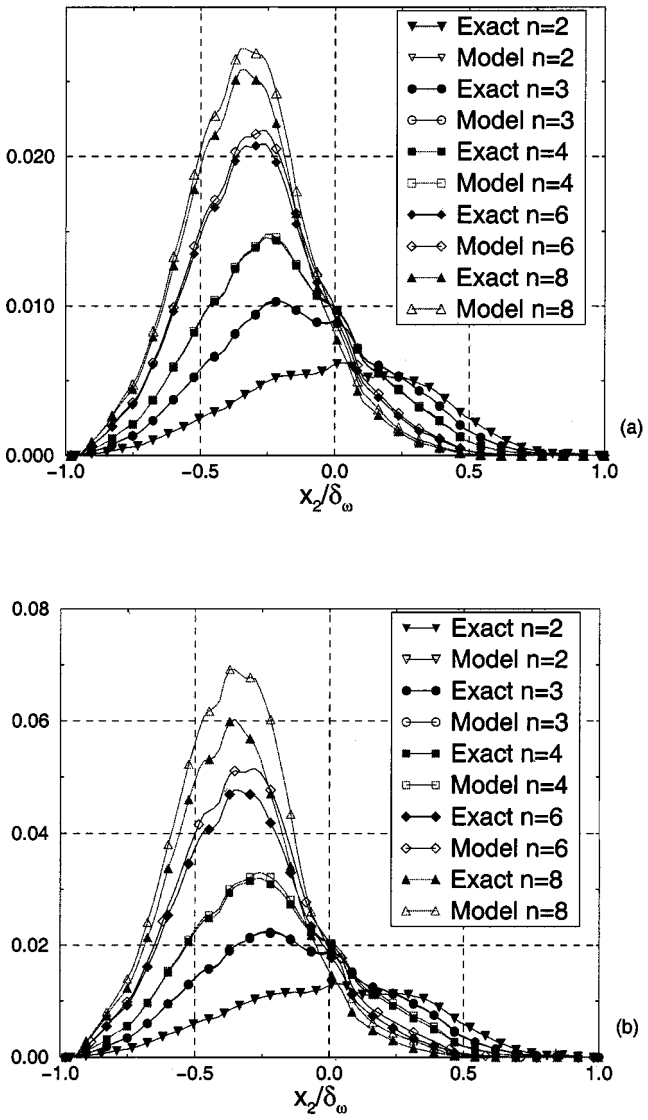

FIG. 2. Exact and model $\langle\overline{Z_{sg}^n}\rangle$, from filtering Z^n. Model with coefficient c_0 obtained from Eq. (37); (a) $\Delta_f/\Delta=4$, (b) $\Delta_f/\Delta=8$.

where Ω in the temporally evolving shear layer considered here is the x_1-x_3 plane of homogeneity. Note that c_0 is a function of the inhomogeneous direction, x_2.

It is important to notice that this is the *best* possible estimate one can get for the coefficient since the fully resolved DNS database is used. Equivalently, the coefficient c_0 can be obtained by solving Eq. (33). Figure 2 show comparisons of the exact and model SGS contribution with coefficient calculated using Eq. (37) for $\Delta_f/\Delta=4$ and 8 and $n=2,3,4,6$, and 8. By construction, the profiles of exact and model terms are identical for $n=2$. As can be seen, the agreement is very good for the higher moments with visible deviations apparently only for $n=6$ and 8. Thus, exactly modeling $\langle\overline{Z_{sg}^2}\rangle$ leads to good prediction of $\langle\overline{Z_{sg}^n}\rangle$ as suggested by the Taylor expansion, Eq. (8).

A second approach, relevant to an actual application of the model where DNS data are unavailable, is to model the spectrum of the scalar field from our knowledge of turbu-

lence physics. The particular turbulent kinetic-energy spectrum[17] is considered here

$$E(\kappa)=C\epsilon^{2/3}\kappa^{-5/3}f_L(\kappa L)f_\eta(\kappa\eta), \tag{38}$$

where κ is the magnitude of the wave number vector

$$f_L(\kappa L)=\left(\frac{\kappa L}{\sqrt{(\kappa L)^2+c_L}}\right)^{5/3+p}, \tag{39}$$

$$f_\eta(\kappa\eta)=e^{-\beta\kappa\eta}, \tag{40}$$

with the parameters $p=4$ and $\beta=5.2$. The wave number is normalized in the model spectrum by the large-scale length scale

$$L=\frac{k^{3/2}}{\epsilon}$$

and the Kolmogorov scale

$$\eta=\left(\frac{\nu^3}{\epsilon}\right)^{1/4}.$$

The constants C and c_L are calculated by requiring that the integrals of $E(\kappa)$ and $2\nu\kappa^2E(\kappa)$ be equal to the turbulent kinetic energy, k, and the turbulent dissipation rate, ϵ, respectively. The spectrum, Eq. (38), has the classical $-5/3$ Kolmogorov scaling in the inertial range, has κ^p scaling for low wave numbers, and exponential decay in the dissipation range. A scalar with molecular Schmidt number $Sc=1.4$, is simulated in the DNS. Therefore, the spectrum of the scalar can be related to that of the turbulent kinetic energy by replacing by η with $\eta_z=\eta Sc^{-1/2}$ where $\eta=(\nu^3/\epsilon)^{1/4}$ is the Kolmogorov scale with ν denoting the molecular viscosity, and $L=L_z=k^{3/2}/\epsilon$ is an integral scale. This permits the definition of a turbulence Reynolds number, $Re_t=k^2/\nu\epsilon$, upon which the spectrum constants depend. The choice of parameters, $p=4$ and $\beta=5.2$, gives a coefficient c_0 that is in good agreement with the calculated from the DNS database, which is at moderate Reynolds number. The value of $p=4$ is in agreement with the expected dependence of the spectrum for low wave numbers,[18] while the value of $\beta=5.2$ is in agreement with experimental results.[17] This spectrum is valid for $Sc\sim1$; for large Schmidt number, a Batchelor spectrum should be used. In terms of the nondimensional variables

$$\vartheta=\kappa L \tag{41}$$

and

$$\mu=\eta_Z/L=Re_t^{-3/4}Sc^{-1/2}, \tag{42}$$

the model spectrum becomes

$$E_Z(\vartheta,\mu)=C_Z\epsilon^{2/3}L^{5/3}\vartheta^{-5/3}f_L(\vartheta)f_\eta(\vartheta\mu), \tag{43}$$

with

$$f_L(\vartheta)=\left(\frac{\vartheta}{\sqrt{\vartheta^2+c_L}}\right)^{5/3+p}, \tag{44}$$

$$f_\eta(\vartheta\mu)=\exp[-\beta(\vartheta\mu)], \tag{45}$$

and $p=4$, $\beta=5.2$. Notice, e.g., from Eq. (33) that the consant $C_Z\epsilon^{2/3}L^{5/3}$ does not play any role in the calculation of the coefficient c_0.

Defining

$$\gamma=\Delta_f/2L, \tag{46}$$

the filter transfer function, Eq. (6), that depends on κ_1, κ_2, and κ_3 is approximated by a spherical function that depends only on $\kappa=|\boldsymbol{\kappa}|$

$$\hat{G}(\vartheta,\gamma)=\frac{\sin(\gamma\vartheta)}{\gamma\vartheta}. \tag{47}$$

Thus, the multidimensional integrals in Eqs. (34)–(36) are simplified to one-dimensional forms which are calculated directly by introducing the model scalar spectrum, Eq. (43), and the filter transfer function, Eq. (47)

$$a_0(\gamma,\mu)=\int_0^\infty E_Z(\vartheta,\mu)[\hat{G}(\vartheta,\gamma)^2-1]\times[1-\hat{G}(\vartheta,\gamma)^2]d\vartheta, \tag{48}$$

$$a_1(\gamma,\mu)=2\int_0^\infty E_Z(\vartheta,\mu)\hat{G}(\vartheta,\gamma)^2[1-\hat{G}(\vartheta,\gamma)]\times[1-\hat{G}(\vartheta,\gamma)^2]d\vartheta, \tag{49}$$

$$a_2(\gamma,\mu)=\int_0^\infty E_Z(\vartheta,\mu)\hat{G}(\vartheta,\gamma)^2[1-\hat{G}(\vartheta,\gamma)]^2\times[1-\hat{G}(\vartheta,\gamma)^2]d\vartheta. \tag{50}$$

The calculated integrals are then inserted into Eq. (33), the quadratic is solved, and the following expression obtained for the model coefficient:

$$c_0=\frac{-a_1(\gamma,\mu)\pm\sqrt{a_1^2(\gamma,\nu)-4a_0(\gamma,\mu)a_2(\gamma,\mu)}}{2a_2(\gamma,\mu)}, \tag{51}$$

where $\mu=\eta_Z/L$ and $\gamma=\Delta_f/2L$. Thus the coefficient, c_0, explicitly depends on how the filter length compares with both the large scale and the small scale in a turbulent flow. Such a dependence can of course be expected on physical grounds. In principle, two values are possible for c_0. The positive branch is selected and this is the value of c_0 that gives the larger pointwise correlation between the exact and model SGS contributions [see Eq. (57) for a definition of the correlation].

Figure 3 shows the variation of the model coefficient as a function of the transverse coordinate in the shear layer at a time when the turbulence is fully developed. The parameters γ and μ have the following values at the center of the shear layer: $\gamma\approx0.086$ and $\mu\approx6\times10^{-3}$. The coefficient tends to its expected value of unity away from the center of the mixing layer, as can be seen in Fig. 3. This is consistent with an improvement of the deconvolution procedure[15] away from the turbulent region where Eq. (13) approaches Eq. (9).

The model scalar spectrum, Eq. (43), can be integrated to give a model (1D) spectrum, $F_\theta(\kappa_1)$. Figure 4(a) shows that the model 1D spectrum is a good fit to the DNS data. However, for robustness of the proposed SGS model re-

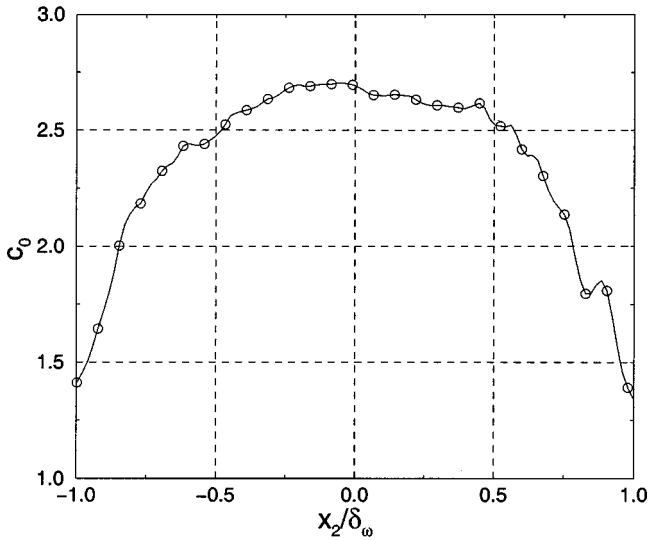

FIG. 3. The behavior of the model coefficient, c_0, as a function of the transverse coordinate in the turbulent shear layer; filter size, $\Delta_f/\Delta=8$.

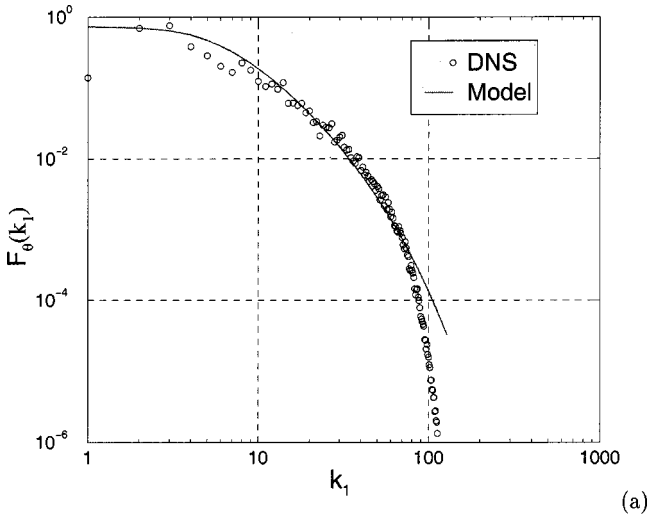

FIG. 4. (a) Comparison of the assumed 1D scalar spectrum to that obtained in DNS; (b) sensitivity of model coefficient c_0 to changes in scalar spectrum parameters c_L and β, when $\Delta_f/\Delta=8$.

quired for more general applications, it is necessary that the model coefficient not be very sensitive to the details of the scalar spectrum. In order to quantify the sensitivity, the consequence of changes in the two parameters, c_L and β, and in the model spectrum, Eq. (43), have been calculated as

$$\Gamma_{c_L}=\frac{1}{c_0}\frac{\partial c_0}{\partial c_L},$$

$$\Gamma_\beta=\frac{1}{c_0}\frac{\partial c_0}{\partial \beta}.$$

Figure 4(b) shows the variation of Γ_{cL} and Γ_β across the shear layer for the case of $\Delta_f/\Delta=8$ obtained with DNS profile of k and ϵ. As can be seen the sensitivities are not large suggesting that the proposed SGS model is indeed robust.

Once the model spectrum, Eq. (43), is fixed, the coefficient c_0 depends on the following parameter: (a) The turbulent Reynolds number, $Re_t=k^2/\nu\epsilon$, (b) Δ_f/L, which is the filter length normalized by a large-scale length scale, L, and (c) the molecular Schmidt number. The turbulent kinetic energy, k, can be estimated by the resolved-scale kinetic energy; the subgrid contribution is typically small. One approach to calculate L is to use the unsteady resolved-scale field. An alternate approach is to use the turbulent dissipation rate, ϵ, calculated as the Reynolds average of its surrogate, the subgrid dissipation, $-\tau_{ij}\overline{s}_{ij}$, where τ_{ij} is the subgrid Reynolds stress and $\overline{s}_{ij}$ is the strain tensor associated with the filtered field.

Thus, for a scalar with a given Schmidt number, c_0 depends on the Reynolds number, Re_t, and the filter size, Δ_f/L. This dependence can be tabulated prior to the LES in an application of the model. Figure 5(a) shows the dependence of the model coefficient on the turbulent Reynolds number for $Sc=1.4$ and $\Delta_f/\Delta=8$. The dependence is weak and appears to be approximately logarithmic. The dependence of c_0 on filter size is shown in Fig. 5(b). A monotone increase with Δ_f/Δ (equivalently, Δ_f/L) is observed.

V. SUMMARY OF THE PROPOSED SUBGRID MODEL

A moment-based reconstruction of the scalar field is formulated. The scalar field is estimated by

$$Z_M=\overline{Z}+c_0(\overline{Z}-\widetilde{Z}), \tag{52}$$

where the single parameter, c_0, is an explicit function, Eq. (51), of the normalized filter size, Δ_f/L, and the normalized Kolomogorov scale, η/L (equivalently the turbulent Reynolds number, Re_t). Such a procedure for calculating c_0 ensures that the average subgrid variance is predicted. The filtered value, $\overline{f(Z)}$, is obtained using Z_M as a surrogate for the scalar field, Z. The problem is usually posed with the objective of modeling the subgrid contribution, $\overline{f(Z)}_{sg}$, defined by Eq. (1), so that the final subgrid model is

$$\overline{f(Z)}_{sg}=\overline{f(Z_M)}-f(\overline{Z}_M). \tag{53}$$

VI. THE DNS DATABASE

The SGS model is evaluated in *a priori* tests using our previous DNS (direct numerical simulation)[19] of the tempo-

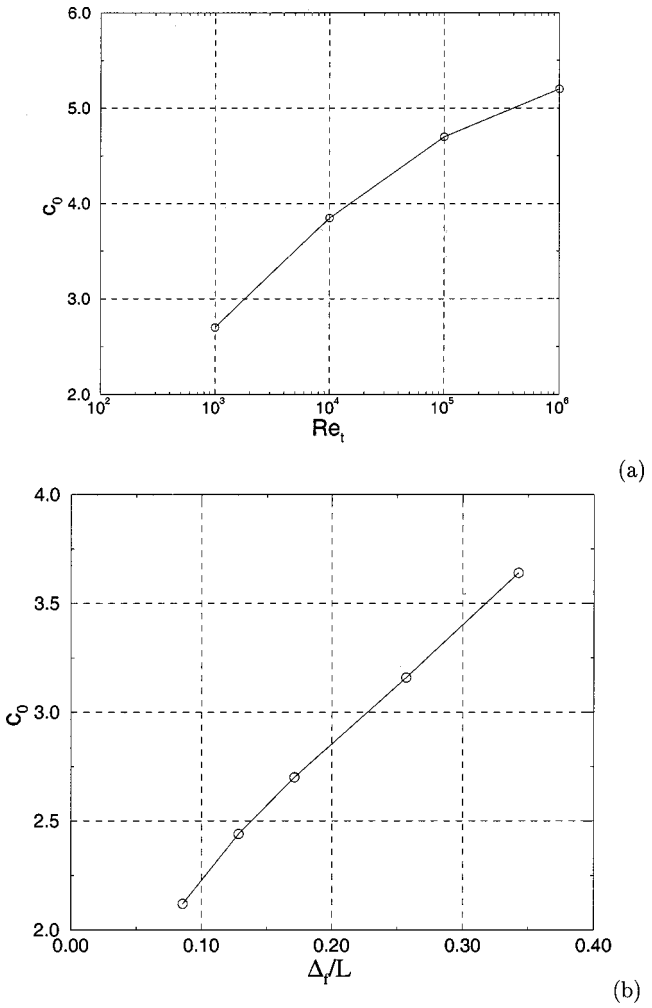

FIG. 5. Dependence of model coefficient on (a) the turbulent Reynolds number when $\Delta_f/L=0.17$, $Sc=1.4$, and (b) the normalized filter size when $Re_t=1000$, $Sc=1.4$.

rally evolving shear layer which has been validated against both experimental work and other DNS. The free-stream value of the scalar is $Z=0$ and $Z=1$ in the upper and lower streams of the shear layer, respectively. In the rest of the paper we will use Z for the scalar normalized by the imposed scalar difference, $\Delta Z=1$. The turbulence is homogeneous in

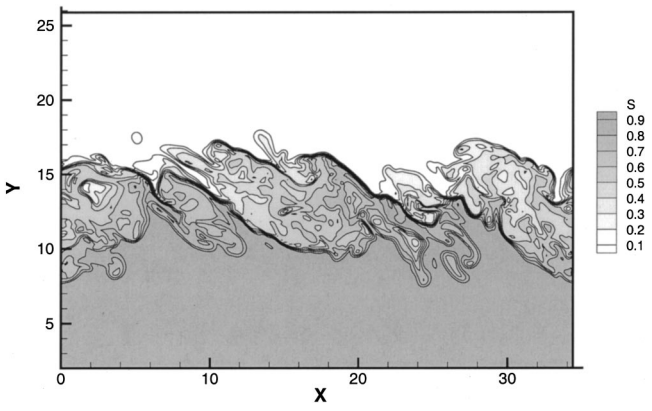

FIG. 6. Instantaneous scalar profile at a vertical cut across the turbulent shear layer $\tau=t\Delta U/\delta_{\omega_0}=323$.

TABLE I. Key parameters of the analyzed field: The Reynolds number based on vorticity thickness δ_ω and Taylor microscale, λ, as well as grid resolution of the vorticity thickness and the Kolmogorov scale, η. The smallest scalar scale is $\eta_s=\eta/\sqrt{Sc}=0.85\eta$.

τ	Re_ω	Re_λ	Δ/δ_ω	Δ/η
323	5684	135	0.018 96	3.36

the x and z directions while the Reynolds-averaged statistics (computed by $x-z$ plane averages) are functions of y and time, t; here (x,y,z) is used interchangeably with (x_1,x_2,x_3). A convective Mach number of $M_c=0.3$ which is small enough to neglect compressibility effects is considered. The DNS database used in the *a priori* tests correspond to a nondimensional time, $\tau=t\Delta U/\delta_{\omega,0}=323$, well into the regime of fully developed turbulence. Here ΔU denotes the velocity difference across the shear layer while $\delta_{\omega,0}$ denotes the initial vorticity thickness of the shear layer. At the centerline, the turbulent Reynolds number, $Re_t=k^2/\nu\epsilon=1000$, while the microscale Reynolds number, $Re_\lambda=q\lambda/\nu=135$. The molecular Schmidt number, $Sc=\nu/D=1.4$ where ν and D are the molecular transport coefficients of momentum and scalar, respectively. A $256\times192\times128$ grid with uniform spatial step size Δ in all directions is used along with fourth-order accurate spatial discretization and third-order Runge–Kutta integration in time.

Figure 6 shows an instantaneous vertical cut of the scalar field across the shear layer. It can be observed that the scalar field is well developed and a wide range of scales are present. Table I summarizes some key parameters of the flow field at this instant; further information on the simulations is available.[19] Figure 7 shows the root-mean-square (r.m.s.) scalar fluctuation, $Z_{\rm rms}=\sqrt{\langle Z^2\rangle-\langle Z\rangle^2}$, as a function of the cross-stream coordinate, y, normalized by the vorticity thickness, $\delta_\omega=\Delta U/(d\langle U\rangle/dy)_{\max}$. The Reynolds average is denoted by $\langle\cdot\rangle$ to distinguish it from the filtering operation.

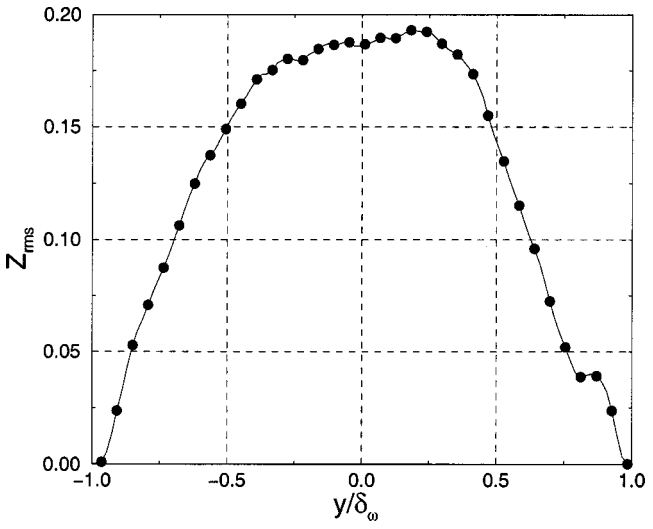

FIG. 7. Profile of the scalar r.m.s. in the fully developed turbulent shear layer; DNS result at $\tau=t\Delta U/\delta_{\omega_0}=323$.

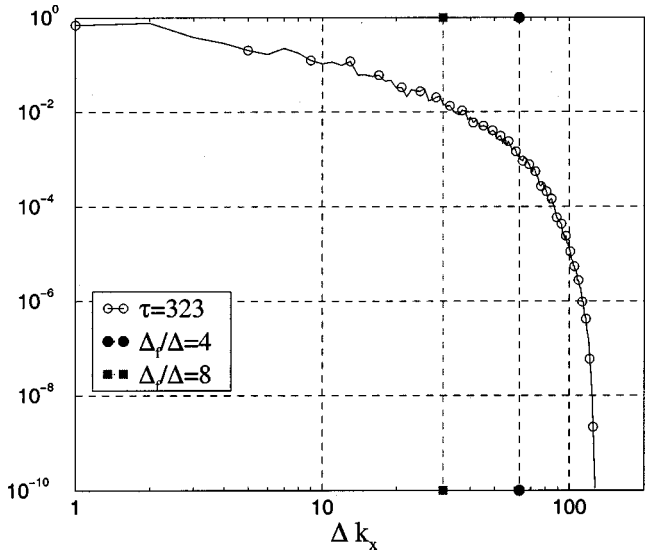

FIG. 8. Spectra in the x-direction at $\tau=323$. The vertical dashed lines with symbols correspond to the filter sizes used here, $\Delta_f/\Delta=4,8$.

VII. SUBGRID SCALE MODEL EVALUATION

The proposed model is based on a moment-based reconstruction procedure and consists of Eq. (53) with the estimated scalar field given by Eq. (52). The performance of the model is assessed using our previous DNS[19] of the temporally evolving shear layer. A late-time field corresponding to fully developed turbulence is used. Two values of the filter size, Δ_f, are used to filter the database in the *a priori* tests. The filter sizes of $\Delta_f/\Delta=4$ and 8 correspond to 12 and 6 points per vorticity thickness, respectively. These are indicated on the scalar spectra shown in Fig. 8. The coefficient, c_0, is obtained using Eq. (51) and the required parameters in the model scalar spectrum, Eq. (43), are evaluated using k and ϵ from the DNS database.

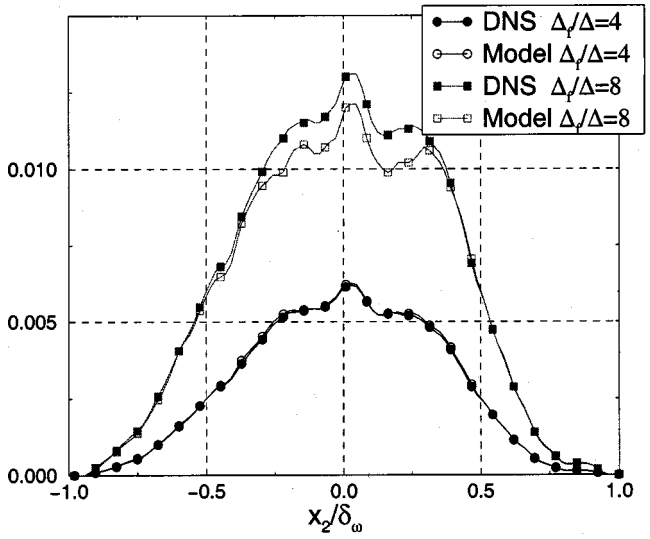

FIG. 9. Performance of model in predicting $\langle\overline{Z_{sg}^2}\rangle$; filter size $\Delta_f/\Delta=4,8$.

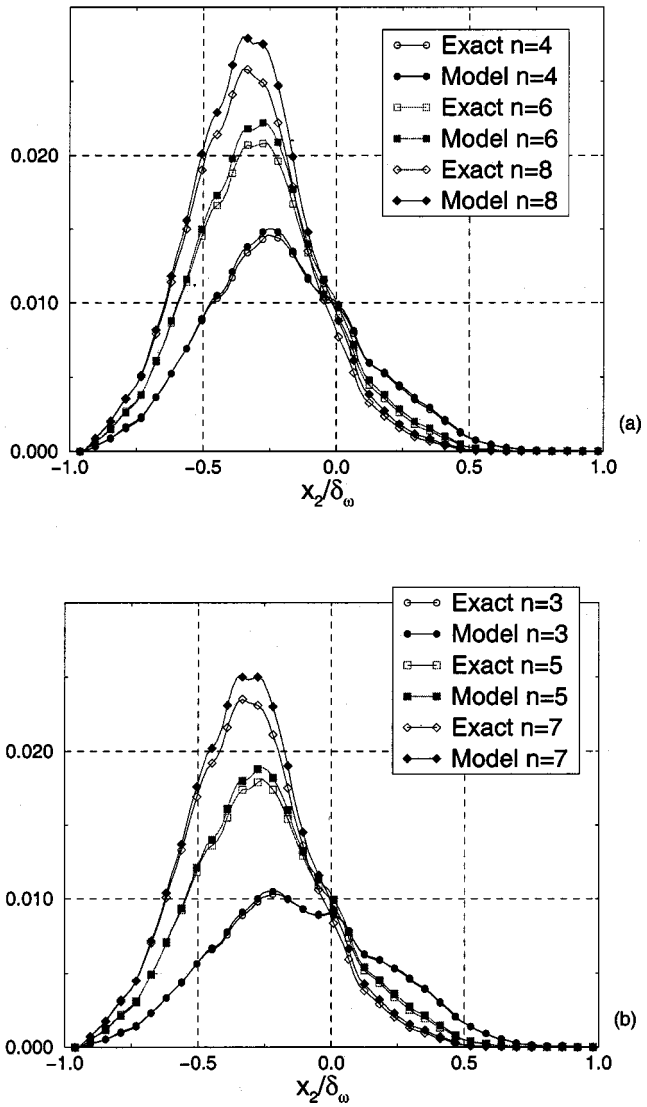

FIG. 10. Performance of the model in predicting the subgrid contribution to various moments of the scalar; filter size $\Delta_f/\Delta=4$.

A. Prediction of algebraic nonlinearity, $\langle\overline{Z_{sg}^n}\rangle$

Profiles of the exact value of $\langle\overline{Z_{sg}^n}\rangle$, an average over the $x-z$ plane of the subgrid contribution

$$\overline{Z_{sg}^n}=\overline{Z^n}-(\overline{Z})^n, \tag{54}$$

are obtained from the DNS database and compared with model predictions. Values of n in the range $2\leqslant n\leqslant 8$ have been used along with various filter sizes.

Figure 9 compares the model with the exact profile of $\langle\overline{Z_{sg}^2}\rangle$. As can be seen, the model is in excellent agreement with the exact values of the averaged SGS contribution. Unlike Fig. 2 where the agreement is exact, there are small differences between exact and predicted values in Fig. 9 because only the model spectrum with k and ϵ as inputs is used for obtaining c_0 instead of the full DNS data.

Figures 10 and 11 shows that the range of moments, Z^n with $n=3-8$, studied here are well-predicted by the model.

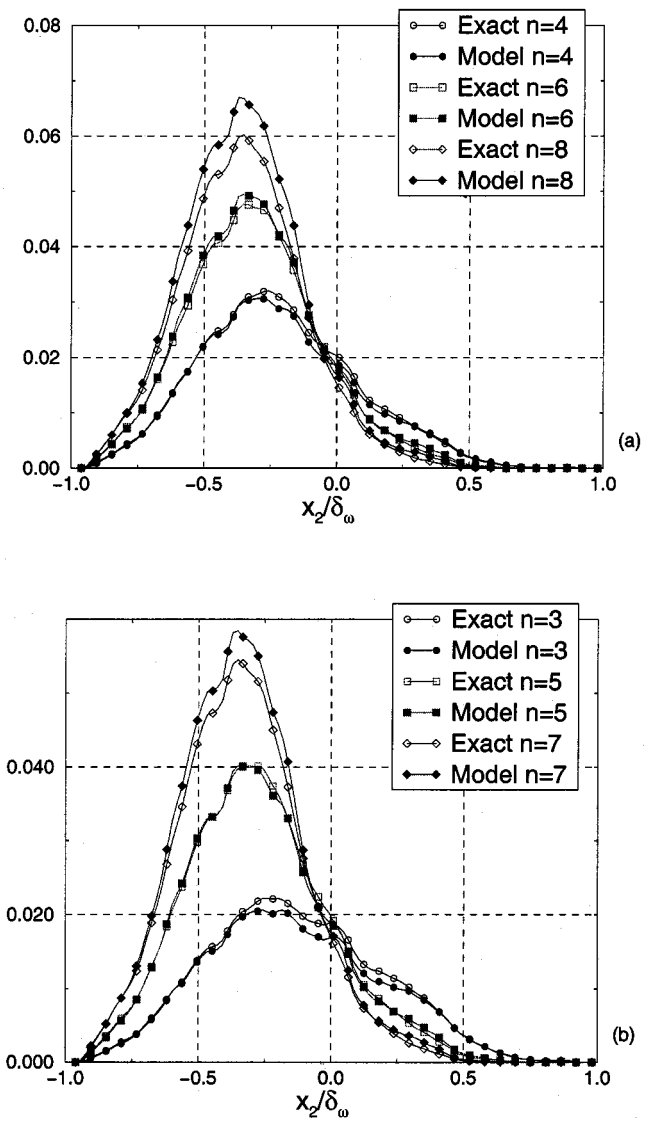

FIG. 11. Performance of the model in predicting the subgrid contribution to various moments of the scalar; filter size $\Delta_f/\Delta=8$.

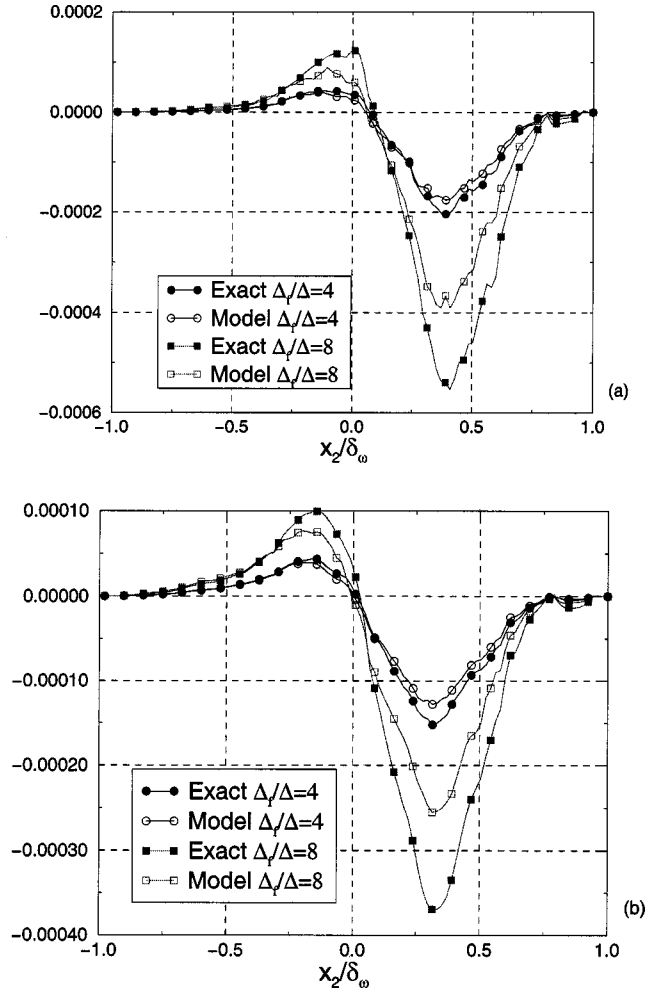

FIG. 12. Exact and model average behavior for an Arrhenius nonlinear function with $T_a=50$, $Z_{st}=0.1$ and $\Delta_f/\Delta=4$ and 8; (a) piecewise temperature profile, Eq. (55), and (b) smooth temperature profile, Eq. (56) with $\delta=0.1$.

The discrepancy between model and exact values increases somewhat with the order of the moment and filter size but always remains less than 10%.

B. Prediction of the Arrhenius nonlinearity, $\langle \overline{e_{sg}^{-T_a/T}} \rangle$

Our intention here is to test the performance of the model for a strongly nonlinear function such as the Arrhenius reaction rate typical of chemical reactions. Consider the nonlinear function $e^{-T_a/T}$, where $T=T(Z)$. Two choices for the mapping between the scalar, Z, and the temperature T are selected. In the first case, a piecewise linear mapping, that corresponds to the Burke–Schumann infinitely fast chemistry approximation, is used,

$$T(Z)=\begin{cases}1+(T_f-1)Z/Z_{st} & \text{if } Z<Z_{st}\\ 1+(T_f-1)(Z-1)/(Z_{st}-1) & \text{if } Z>Z_{st}\end{cases}, \quad (55)$$

where T_f is the adiabatic flame temperature and Z_{st} is the stoichiometric value of the mixture fraction. The reference cold temperature is normalized to unity in both freestreams. Equation (55) is chosen so as to realize a temperature field associated with a system with fast chemistry; it is recognized that, in the infinitely fast limit, the overall rate is determined by the scalar and the conditional scalar dissipation,[20] but rates of production of trace species such as oxides of nitrogen can have this Arrhenius form, in this limit. In the second case, the temperature gradient across the flame, $Z=Z_{st}$, is smoothed out by the use of a hyperbolic tangent profile[21] connecting the values of dT/dZ in the upper and lower streams as follows:

$$\frac{dT}{dZ}=(T_f-1)\left\{\frac{1}{Z_{st}}+\frac{1}{2Z_{st}(Z_{st}-1)}(1+\tanh((Z-Z_{st})/\delta))\right\}. \quad (56)$$

Here δ is a smoothing factor. Furthermore, the model scalar is limited to $0\leqslant Z_M\leqslant 1$ to satisfy the natural constraints of the scalar field.

Results for $Z_{st}=0.1$, $T_f=10$, $T_a=50$ and $\delta=0.1$ are shown for filter sizes $\Delta_f/\Delta=4$ and 8 in Figs. 12(a) and 12(b). These values are representative of some hydrocarbon-air combustion problems. Both choices for the temperature dependence on the scalar, a piecewise linear profile, Eq.

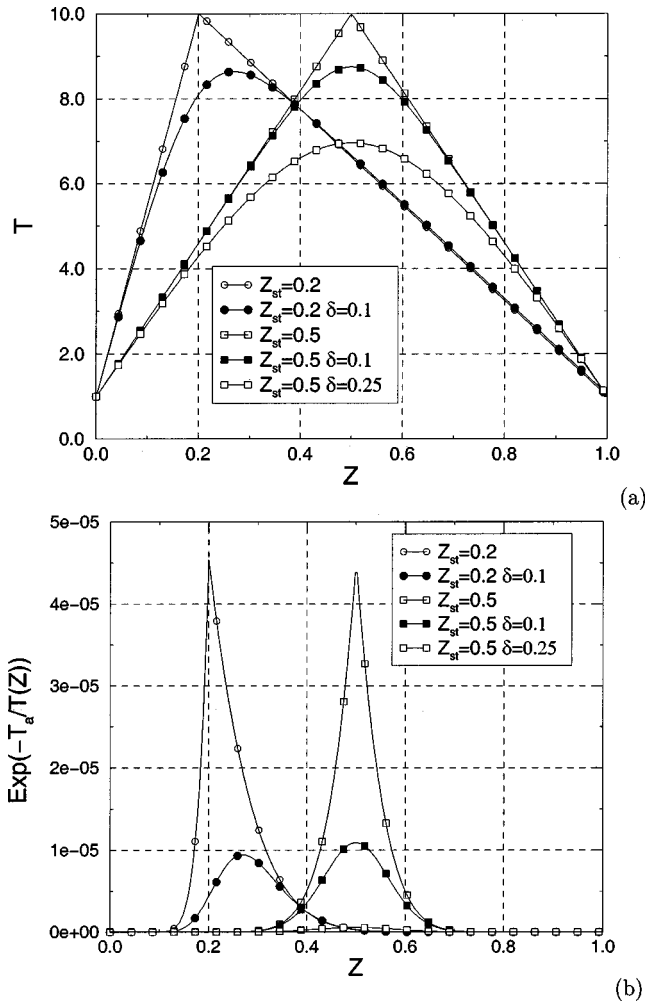

FIG. 13. (a) Various choices of the functional depepndence of temperature on mixture fraction in the SGS model evaluations, (b) the corresponding Arrhenius term. The adiabatic flame temperature is $T_f=10$ while the activation energy temperature is $T_a=100$.

(55), and a smoothed profile, Eq. (56), lead to the same trend: the model prediction is very good for $\Delta_f/\Delta=4$ but, when the filter size is $\Delta_f/\Delta=8$, the model underpredicts the subgrid peak contribution by about 35%.

Calculations have been performed for a wider range of parameters to further investigate the model behavior in the case of the larger filter size, $\Delta_f/\Delta=8$. The choice of activation energy temperature, $T_a=100$ and the flame temperature, $T_f=10$ correspond to chemistry representative of large activation energy typical of hydrocarbons. Two values of the stoichiometry, $Z_{st}=0.2$ and 0.5, and two values of the smoothing factor of the temperature profile, $\delta=0.1$ and 0.25, are used. Figure 13(a) shows the different functional dependences of the temperature profile on the mixture fraction while Fig. 13(b) shows the corresponding Arrhenius nonlinearity.

Figure 14 shows the effect of stoichiometric mixture fraction on the behavior of the model for the large filter size. It can be seen that the agreement is better for $Z_{st}=0.5$, when the average location of the flame is at the center of the mixing layer. When $Z_{st}=0.2$, the prediction follows the shape of the exact profile; however, there is underprediction of the

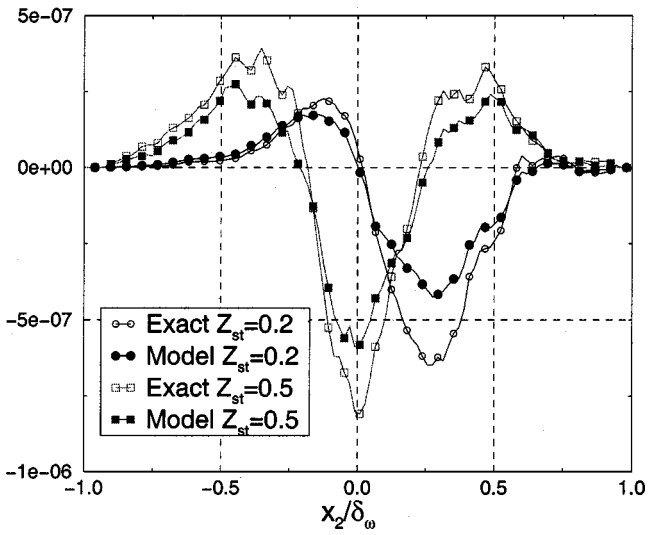

FIG. 14. Influence of Z_{st} on the model behavior. Arrhenius nonlinear function with $T_a=100$, $T_f=10$, and smooth temperature profile with $\delta=0.1$. The filter size is $\Delta_f/\Delta=8$.

peak similar in magnitude to that in the case with $Z_{st}=0.1$. Potential reasons for the difference between model predictions and exact values that occurs when Z_{st} departs from the value, 0.5, are the more intermittent mixing events at the edge of the shear layer resulting in larger subgrid fluctuations as well as the increased nonlinearity of the scalar dependence, see Fig. 13.

Figure 15 shows the effect of the smoothing factor associated with the temperature profile, δ, for $Z_{st}=0.5$. When the profile becomes sharper (smaller value of δ) the contribution of the subgrid term increases. The model performance remains very good even for sharper $T(Z)$ profiles.

C. Instantaneous performance of the SGS model

Figure 16 shows a scatter plot of the exact versus the model SGS contribution for $n=2$ and $\Delta_f/\Delta=8$ calculated at

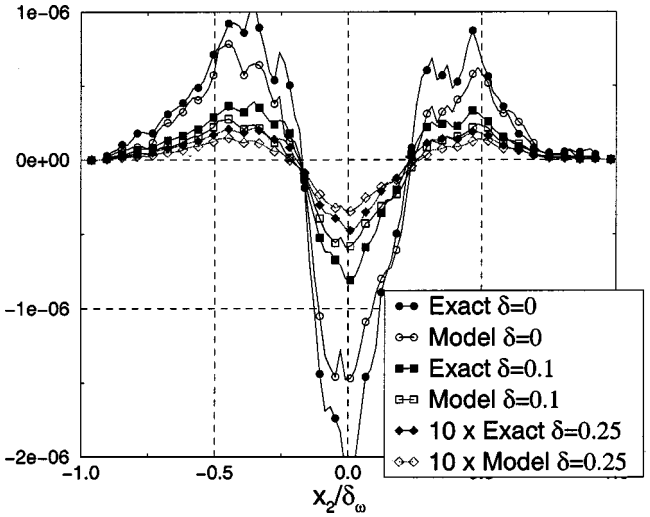

FIG. 15. Influence of the smoothing factor δ in the temperature profile. Arrhenius nonlinearity with $T_a=100$, $T_f=10$, $Z_{st}=0.5$, and filter size $\Delta_f/\Delta=8$.

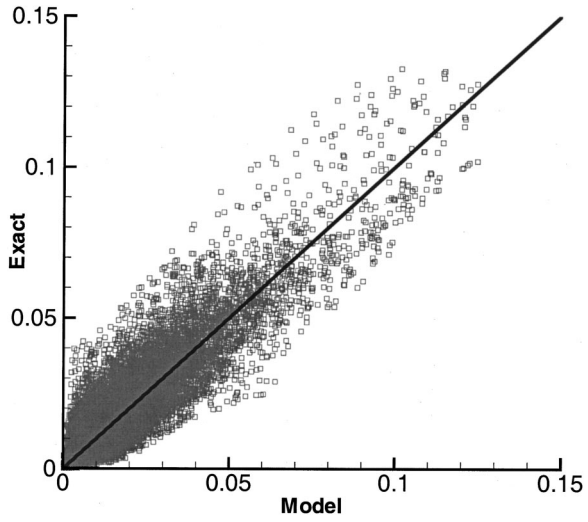

FIG. 16. Scatter of the model prediction with respect to the exact subgrid contribution to the filtered value of Z^2; $\Delta_f/\Delta=8$.

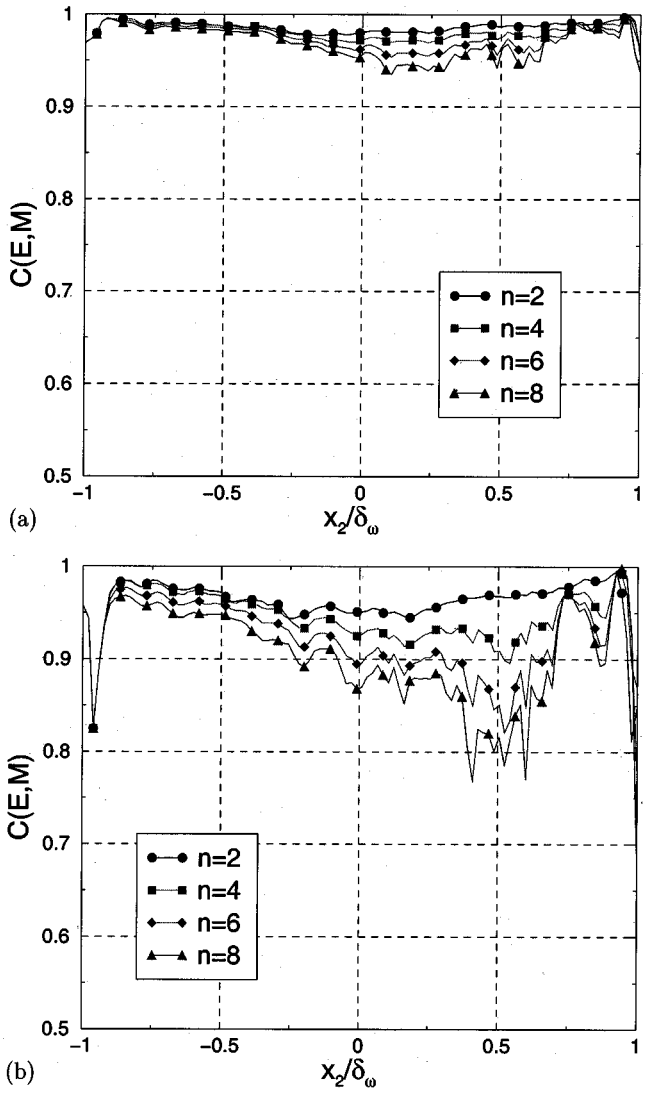

FIG. 17. Correlation between exact and model SGS contribution for polynomial nonlinear function, Z^n, with $n=2,4,6,8$ as a function of self-similar coordinate, for (a) $\Delta_f/\Delta=4$ and (b) $\Delta_f/\Delta=8$ and later time, $\tau=t\Delta U/\delta_{\omega 0}=323$.

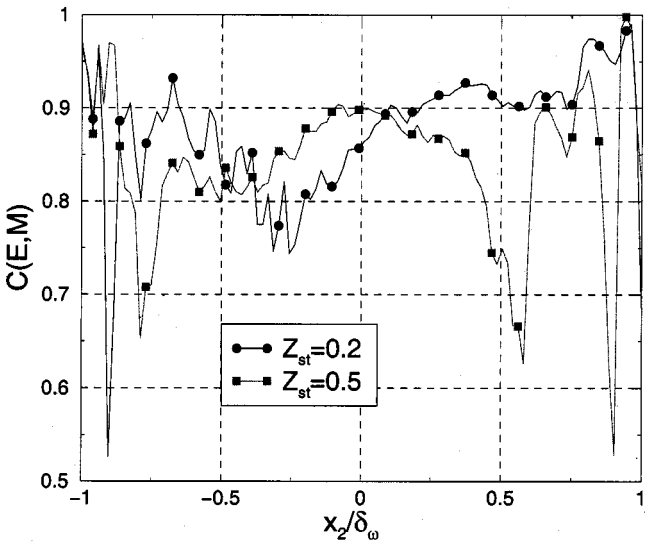

FIG. 18. Correlation between exact and model SGS contribution for Arrhenius nonlinear function, with $T_a=100$, $T_f=10$, and two choices for the stoichiometric mixture fraction, $Z_{st}=0.2$ and 0.5 as a function of self-similar coordinate, for $\Delta_f/\Delta=8$.

the mixing layer centerplane. As can be seen there is some scatter. Scatter is *not surprising* since there is statistical unpredictability of the subgrid values of the scalar even if the exact filtered field is available. Furthermore, the single-parameter model tested here is the simplest-possible case that guarantees only the prediction of the second moment of the subgrid contribution. The amount of scatter could perhaps be improved if a more complex model and/or a different optimization technique is used in the calculation of the coefficients.

To further examine the model we investigate the behavior of the correlation coefficient between the exact and model SGS contributions defined by

$$C(E,M)=\frac{\langle \overline{f(Z_M)}_{sg}\,\overline{f(Z)}_{sg}\rangle}{\sqrt{\langle \overline{f(Z_M)}^2_{sg}\rangle\langle \overline{f(Z)}^2_{sg}\rangle}}. \tag{57}$$

Figures 17(a) and 17(b) shows the behavior of the correlation coefficient for the polynomial nonlinear function, Z^n, as a function of the self-similar coordinate. It can be seen that the correlation coefficient is very high when $\Delta_f/\Delta=4$ for all values of n considered here, with a value above 0.94. For $\Delta_f/\Delta=8$, the correlation, although lower than in the previous case, remains good. The minimum value of the correlation coefficient is 0.8 and occurs for $n=8$.

Finally, Fig. 18 shows the correlation coefficient for the Arrhenius nonlinear function with $T_a=100$, $T_f=10$, and two choices for the stoichiometric mixture fraction, $Z_{st}=0.2$ and 0.5 as a function of self-similar coordinate, for $\Delta_f/\Delta=8$. The correlation coefficient is above 0.8 in most of the shear layer.

Figures 19 and 20 show instantaneous contour plots of the exact and model SGS contribution for a filter size of $\Delta_f/\Delta=8$ and moments with $n=2$ and 8 at the center plane. The model is capable of capturing the structural characteristics in both cases very well.

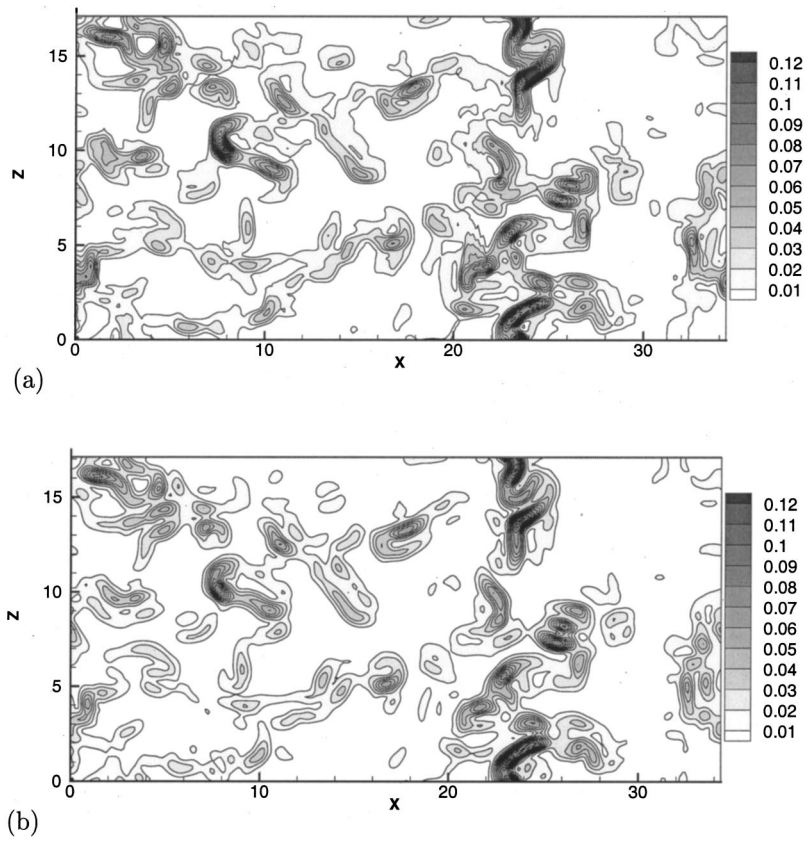

FIG. 19. Contour plots $\overline{Z_{sg}^2}$ in the centerplane, $\Delta_f/\Delta = 8$. (a) Exact, and (b) model prediction.

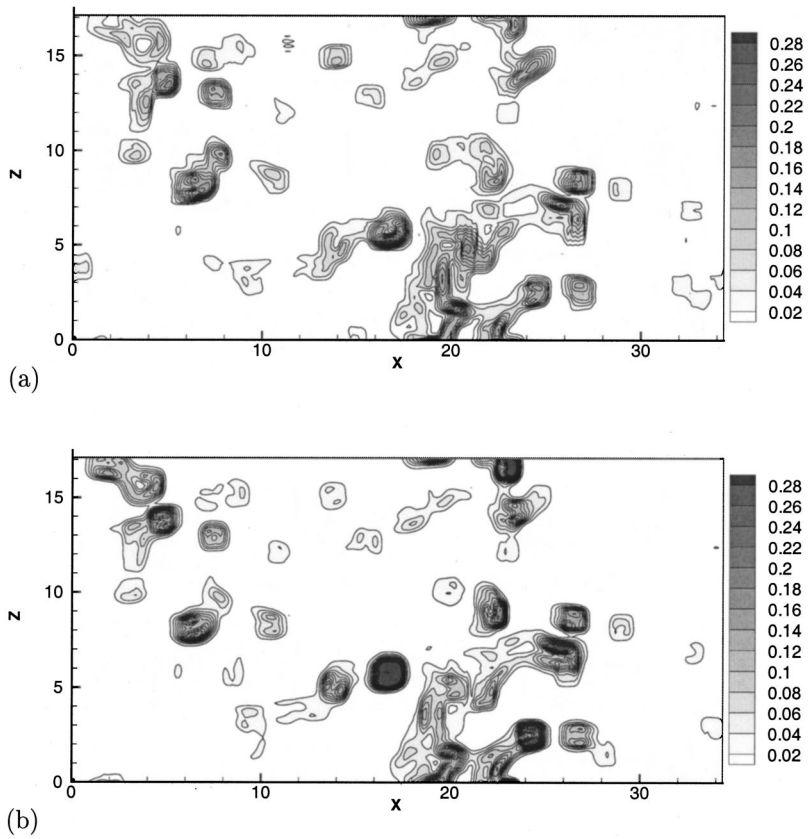

FIG. 20. Contour plots $\overline{Z_{sg}^8}$ in the centerplane, $\Delta_f/\Delta = 8$. (a) Exact, and (b) model prediction.

VIII. CONCLUSIONS

In applications of LES such as radiation heat transfer and combustion, models are required for strongly nonlinear functions, $f(Z)$, of a scalar Z. A moment-based reconstruction procedure to model the subgrid contribution to the filtered value, $\overline{f(Z)}$, is proposed here. In this methodology, the scalar field is estimated by an approximate deconvolution operation, Eq. (52), and the estimated scalar field is used as a surrogate for the exact field in the calculation of the subgrid contribution by Eq. (53). Unlike the usual deconvolution operation with given coefficients, the coefficients in the expansion are allowed to be variable and instead obtained by requiring that the statistical moments of the scalar field up to a certain order are matched. The usual deconvolution operation is not adopted because substantial errors in predicting the subgrid scalar variance are found in *a priori* tests using a turbulent shear-layer database. A Taylor series expansion of the nonlinear function of Z around its filtered value of Z motivates our *ansatz* of matching subgrid moments to determine the unknown coefficient.

The simplest possible form of the moment-based reconstruction, one that involves a single unknown parameter so that the average subgrid contribution to $\overline{Z^2}$ is matched by the estimated scalar field, is evaluated using our DNS database of a turbulent shear layer. Two filter sizes are tested: $\Delta_f/\Delta = 4$ corresponding to 12 points per vorticity thickness, and $\Delta_f/\Delta = 8$ corresponding to 6 points per vorticity thickness.

The single coefficient, c_0, involved in the proposed model, Eq. (52), depends on the scalar spectrum. A simple model spectrum is found to be sufficient to estimate the coefficient and give an excellent prediction of the averaged subgrid variance; furthermore, the sensitivity of the coefficient to the two parameters embedded in the model spectrum is found to be small. Thus, additional input of turbulence physics via the scalar spectrum is necessary to match the average value of the subgrid contribution to $\overline{Z^2}$; simple reconstruction from the filtered field is not sufficient in this problem. The chosen model spectrum which has Kolmogorov scaling in the inertial range leads to the physically appealing result that the model coefficient is a function of how large the filter length scale, Δ_f, is in relation to both the large-scale length scale, L, and the small-scale Kolmogorov scale, η_Z. In an LES application, the dependence of c_0 on Δ_f/L, and η_Z/Δ_f (equivalently, the turbulence Reynolds number, Re_t) can be tabulated prior to the calculation.

The model spectrum used here has Kolmogorov inertial range scaling and dissipation range scaling typical of incompressible turbulence. In more general situations, other effects on the unresolved scales such as compressibility and rotation could become important. In such situations, the assumed scalar spectrum would be different and would have to be chosen appropriately based on knowledge of turbulence physics.

Functions with polynomial nonlinearities are first tested with respect to prediction of the profile of average subgrid contribution in the shear layer. It is found that, for both filter sizes, the single-parameter model performs well over the wide range of functions tested here, Z^n with $n=3,...,8$. Thus, our *ansatz* that matching moments of lower-order nonlinearities, $\langle\overline{Z_{sg}^2}\rangle$ in this instance, leads to good results for high-order nonlinearities appears to be valid in this problem. This is encouraging for LES applications that involve functions with a polynomial nonlinearity such as the T^4 dependence in radiation heat transfer as well as the species and temperature dependence on the mixture fraction in solutions of the strained laminar flamelet model.

The pointwise values of the modeled subgrid-scale contribution to $\overline{Z^n}$ show scatter with respect to the exact values. This scatter is to be expected because of the unpredictability of the small-scale motion giving only the filtered field.

The Arrhenius nonlinearity in the reaction rate is a more challenging problem because the ratio of activation temperature to flame temperature is typically a large number of $O(10)$. It is found that the model works well for a diluted hydrocarbon system with stoichiometric mixture fraction, $Z_{st}=0.5$, corresponding to the average flame location being in the turbulent core of the shear layer. For typically more realistic mixture fractions of $Z_{st}=0.1, 0.2$, the finer-resolution application of our proposed model gives good results with less than 10% deviation. The coarse-resolution application with 6 points per vorticity thickness gives profiles of the averaged filtered contribution that follow the exact profile; however, there is underprediction of the peak contribution to the subgrid reaction rate by up to 35%. Note that the coarser filter size corresponds to a very stringent test; even a Reynolds-averaged closure typically uses such a resolution or better. Even so, future refinements to improve model performance with such coarse grids are desirable. Furthermore, investigation of the effect of using a coarse LES grid with respect to a fine DNS grid shows that keeping the numerical grid finer than that used for defining the filtered field ensures that the model performance does not deteriorate due to numerical resolution.

Further tests of the proposed model are reported in the Appendix. The case of a more general model, where a test filter, wider than the main filter, is used for the second filtering operation is considered. The results are found to be in agreement with the case of equal test and main filters if the calculation of the model parameter, c_0, is done consistently. In LES applications, the grid resolution is coarse relative to that used to generate the DNS database. It is found that, if the LES grid size is larger than twice the filter size, the effect of coarse grid discretization is negligible.

ACKNOWLEDGMENTS

We thank F. A. Williams for discussions of this research and for comments on the manuscript. The research was partially supported by AFOSR Grant No. F49620-96-1-0106, and under the auspices of DOE by LLNL under Contract No. W-7405-ENG-48. Computational time was provided at the NAVO Major Shared Resource Center through an HPCMP allocation and the San Diego Supercomputer Center through an NPACI allocation.

APPENDIX: ADDITIONAL *A PRIORI* TESTS

The *a priori* tests using our DNS calculation use the full, highly-resolved data set so that the SGS model can be tested separate from considerations of numerical resolution. However, in an actual LES calculation, the SGS contribution has to be evaluated from the available filtered field represented on a grid that contains fewer points than the number of points necessary for a fully resolved field. The lack of information that results from the use of a coarse-grid representation of the data can be incorporated in a modified *a priori* test wherein the filter transfer function, $\hat{G}(\kappa)$, is replaced by $\hat{G}(\kappa)H(\kappa_g-\kappa)$ in Eqs. (34)–(36), where $H(\kappa_g-\kappa)$ is the unitary step function (unity for $\kappa<\kappa_g$ and zero for $\kappa\geqslant\kappa_g$), and κ_g is the cutoff wave number associated with the coarse grid.

The performance of the proposed model, Eq. (17), was gauged in the main body of the paper with the main (bar) filter and test (tilde) filters assumed to be the same. However, there are situations where the test filter should have a larger characteristic length than the main filter. One such situation, that occurs in many practical applications of LES, is when the grid size for the LES is taken to be the same as the size of the tophat filter. When a spectral cutoff filter is used instead of a tophat filter, it is again necessary to distinguish between the main and test filters because $\overline{Z}=\tilde{\bar{Z}}$ giving $Z_M=\overline{Z}$. The model, Eq. (17), has the following transfer function:

$$\hat{M}_1=\hat{G}(\kappa)H(\kappa_g-\kappa)[1+c_0(1-\hat{G}_t(\kappa)H(\kappa_g-\kappa))], \tag{A1}$$

where $\hat{G}_t(\kappa)$ is the transfer function of the test filter. Notice that the test filter does not need to be of the same type as the implicit LES filter.

To further explore the properties of the proposed one-parameter model, we study the effect of the test filter and a

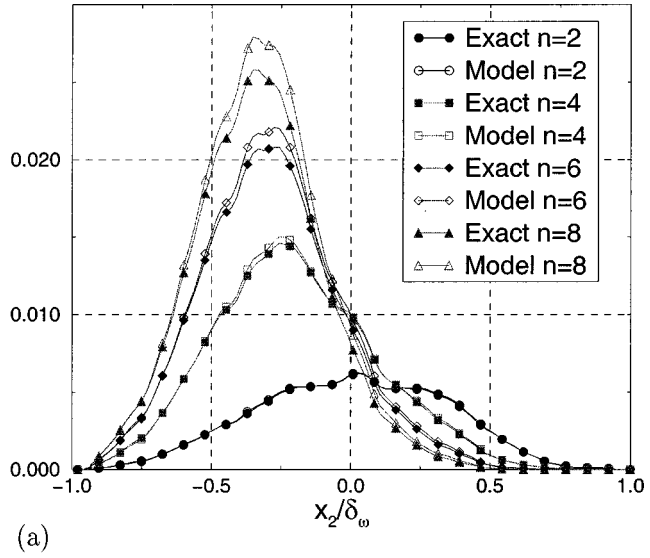

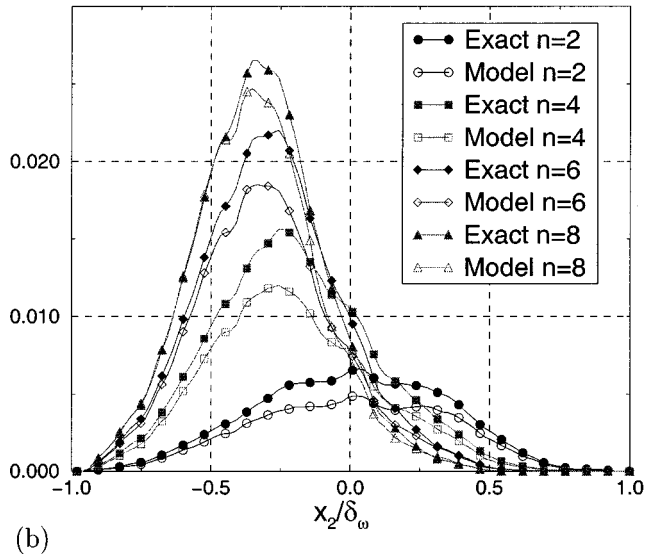

FIG. 21. Effect of numerical grid resolution on model performance; $\Delta_f/\Delta=4$ and (a) $\Delta_g=\Delta_f/2$ and (b) $\Delta_g=\Delta_f$ and later time, $\tau=t\Delta U/\delta_{\omega 0}=323$.

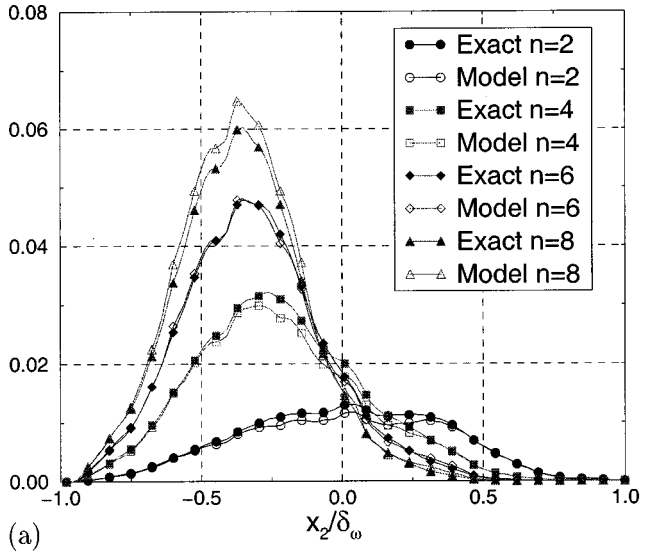

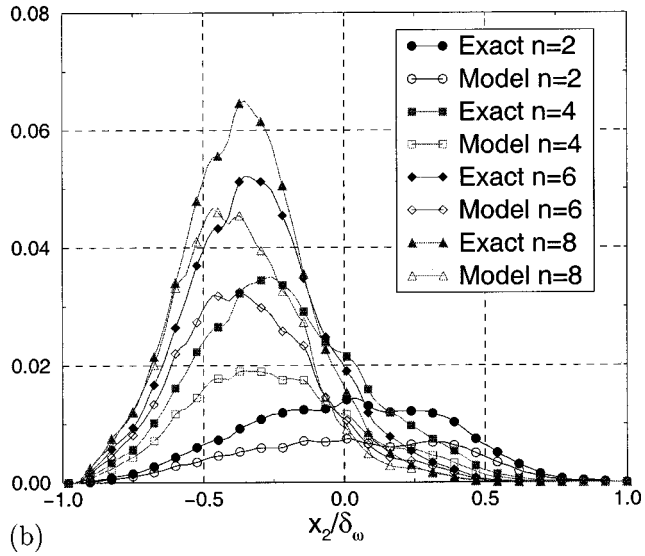

FIG. 22. Effect of numerical grid resolution on model performance; $\Delta_f/\Delta=8$ and (a) $\Delta_g=\Delta_f/2$ and (b) $\Delta_g=\Delta_f$ and later time, $\tau=t\Delta U/\delta_{\omega 0}=323$.

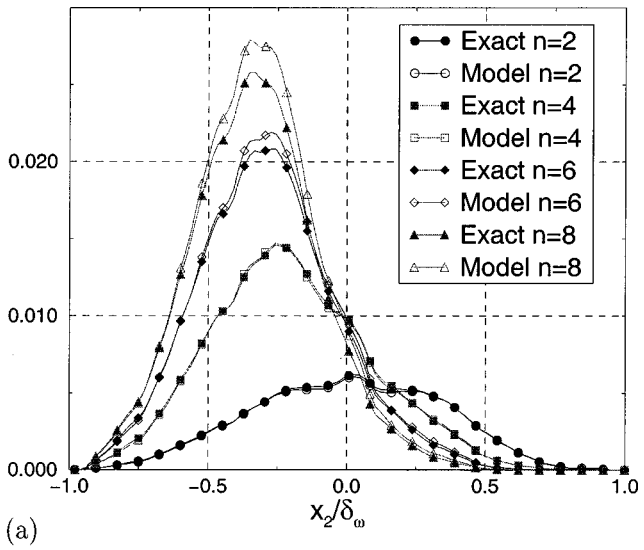

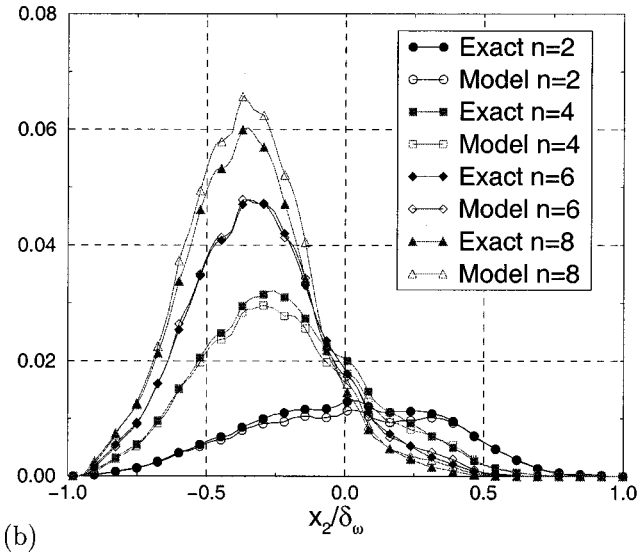

FIG. 23. Performance of model when the test filter is not the same as the main filter; $\Delta_t = 2\Delta_f$ for (a) $\Delta_f/\Delta = 4$ and (b) $\Delta_f/\Delta = 8$ and later time, $\tau = t\Delta U/\delta_{\omega 0} = 323$.

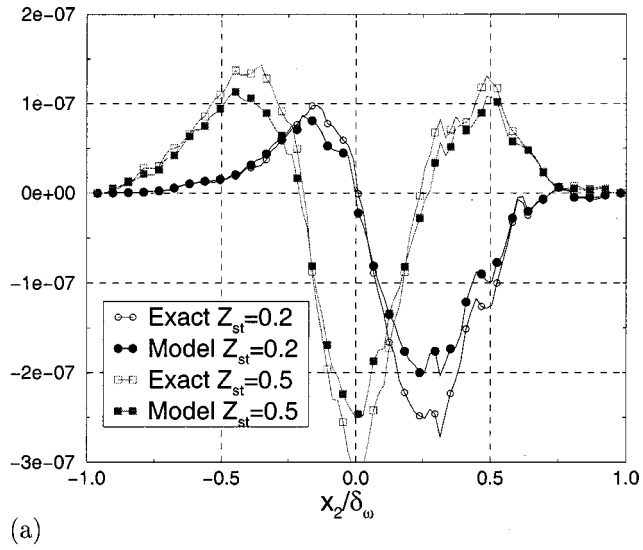

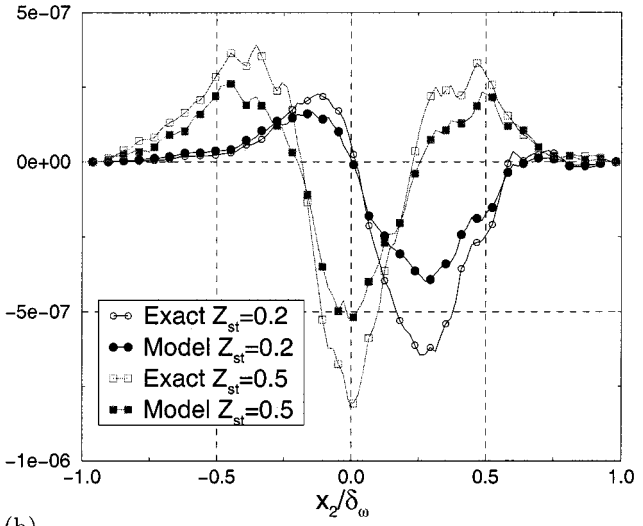

FIG. 24. Performance of the model, Eq. (17) for an Arrhenius nonlinear function with $T_a = 100$, $T_f = 10$, and two choices for the stoichiometric mixture fraction, $Z_{st} = 0.2$ and 0.5. The test filter is $\Delta_t = 2\Delta_f$ while the grid filter is $\Delta_g = \Delta_f/2$. Two choices of the main filter are shown: (a) $\Delta_f/\Delta = 4$ and (b) $\Delta_f/\Delta = 8$.

coarse grid in the performance of the model. For consistency with Sec. IV B, the main filter, grid discretization filter, and test filter are parameterized by their widths, Δ_f, Δ_g, and Δ_t, respectively. In the model performance calculations that are presented below, the model coefficient, c_0, is calculated taking into account Eq. (A1). The new set of coefficients, a_i, to be used in Eq. (33) are

$$a_0 = \int_{-\infty}^{\infty} E_Z(\boldsymbol{\kappa}_0)[\hat{G}(\boldsymbol{\kappa}_0)\hat{G}^*(\boldsymbol{\kappa}_0)H(\kappa_g - \kappa_0) - 1] \times [1 - \hat{G}(\boldsymbol{\kappa}_0)\hat{G}^*(\boldsymbol{\kappa}_0)H(\kappa_g - \kappa_0)]d\boldsymbol{\kappa}_0, \quad \text{(A2)}$$

$$a_1 = \int_{-\infty}^{\infty} E_Z(\boldsymbol{\kappa}_0)\hat{G}(\boldsymbol{\kappa}_0)\hat{G}^*(\boldsymbol{\kappa}_0)H(\kappa_g - \kappa_0) \times [2 - \hat{G}_t(\boldsymbol{\kappa}_0) - \hat{G}_t^*(\boldsymbol{\kappa}_0)][1 - \hat{G}(\boldsymbol{\kappa}_0)\hat{G}^*(\boldsymbol{\kappa}_0)]d\boldsymbol{\kappa}_0, \quad \text{(A3)}$$

$$a_2 = \int_{-\infty}^{\infty} E_Z(\boldsymbol{\kappa}_0)\hat{G}(\boldsymbol{\kappa}_0)\hat{G}^*(\boldsymbol{\kappa}_0)H(\kappa_g - \kappa_0)[1 - \hat{G}_t(\boldsymbol{\kappa}_0)] \times [1 - \hat{G}_t^*(\boldsymbol{\kappa}_0)][1 - \hat{G}(\boldsymbol{\kappa}_0)\hat{G}^*(\boldsymbol{\kappa}_0)]d\boldsymbol{\kappa}_0. \quad \text{(A4)}$$

The filtered field, $\overline{Z}$, and test-filtered field, $\widetilde{Z}$, are obtained after processing the field that results after a spectral cutoff filter, with a cutoff wave number κ_g corresponding to the numerical grid size, is applied to the DNS dataset.

1. Effect of grid resolution

A priori evaluation of the model is performed for polynomial nonlinear functions, Z^n, with $n = 2,4,6$, and 8. Odd powers of n, are not shown for brevity since the results are similar to the ones obtained for the even powers. Two filter widths are tested: $\Delta_f/\Delta = 4$ and 8 with the test filter identical

to the main filter. Figures 21(a) and 21(b) show the performance of the model for $\Delta_f/\Delta=4$ and $\Delta_g=\Delta_f/2$ and $\Delta_g=\Delta_f$, respectively. It can be observed that the case with $\Delta_g=\Delta_f/2$ shows better prediction of the mean SGS contribution for n up to 6 in comparison with the case $\Delta_g=\Delta_f$ and about the same agreement for $n=8$. This is no longer true for the case with $\Delta_f/\Delta=8$ shown in Figs. 22(a) and 22(b). Now, while the case $\Delta_g=\Delta_f/2$ shows good agreement for all powers, the same cannot be said for $\Delta_g=\Delta_f$ where degradation of the model results are observed.

The overall conclusion is that keeping the numerical grid finer than that used for defining the filtered field ensures that the model performance does not deteriorate due to numerical resolution. In particular, the results suggest that a safe choice during application of the model is $\Delta_g=\Delta_f/2$.

2. Effect of test filter

To further investigate the combined effect of grid resolution and test filter, the performance of the model is studied again for the polynomial nonlinear function Z^n with a test filter that is not identical to the main filter. Figures 23(a) and 23(b) show the performance of the model for $\Delta_t=2\Delta_f$ and $\Delta_g=\Delta_f/2$ for two different filter sizes, $\Delta_f/\Delta=4$ and $\Delta_f/\Delta=8$. The choice of $\Delta_g=\Delta_f/2$ is guided by results of the previous section indicating that $\Delta_g=\Delta_f/2$ is sufficient to avoid deleterious effects of numerical grid resolution. It is observed that the model produces results that are in excellent agreement with the exact values calculated from the DNS database.

For completeness, the case of an Arrhenius nonlinear function is shown for $\Delta_t=2\Delta_f$ and $\Delta_g=\Delta_f/2$ for two different filter sizes, $\Delta_f/\Delta=4$ and $\Delta_f/\Delta=8$ in Figs. 24(a) and 24(b). Similar to the results discussed in the main body of the paper, the agreement is better for the smaller filter size.

[1]F. A. Williams, *Combustion Theory* (Addison-Wesley, Reading, MA, 1985).
[2]N. Peters, ''Laminar flamelet concepts in turbulent combustion,'' Twenty-first Symposium (International) on Combustion (1986), p. 1231.
[3]A. R. Kerstein, ''A linear-eddy model of turbulent scalar transport and mixing,'' Combust. Sci. Technol. **60**, 391 (1988).
[4]P. A. McMurtry, S. Menon, and A. R. Kerstein, ''Linear eddy modeling of turbulent combustion,'' Energy Fuels **7**, 817 (1993).
[5]W. W. Kim, S. Menon, and H. C. Mongia, ''Large-eddy simulation of a gas turbine combustor flow,'' Combust. Sci. Technol. **143**, 25 (1999).
[6]C. K. Madnia and P. Givi, ''Direct numerical simulation and large eddy simulation of reacting homogeneous turbulence,'' in *Large Eddy Simulation of Complex Engineering and Geophysical Flows*, edited by B. Galperin and S. A. Orszag (Cambridge University Press, Cambridge, 1993).
[7]A. W. Cook and J. J. Riley, ''A subgrid model for equilibrium chemistry in turbulent flows,'' Phys. Fluids **6**, 2868 (1994).
[8]A. W. Cook, ''Determination of the constant coefficient in scale similarity models of turbulence,'' Phys. Fluids **9**, 1485 (1997).
[9]C. D. Pierce and P. Moin, ''A dynamic model for subgrid-scale variance and dissipation rate of a conserved scalar,'' Phys. Fluids **10**, 3041 (1998).
[10]A. W. Cook, J. J. Riley, and G. Kosaly, ''A laminar flamelet approach to subgrid-scale chemistry in turbulent flows,'' Combust. Flame. **109**, 332 (1997).
[11]J. Jiménez, A. Liñán, M. M. Rogers, and F. J. Higuera, ''A priori testing of subgrid models for chemically reacting non-premixed turbulent shear flows,'' J. Fluid Mech. **349**, 149 (1997).
[12]P. E. DesJardin and S. H. Frankel, ''Large eddy simulation of a nonpremixed reacting jet: Application and assessment of subgrid-scale combustion models,'' Phys. Fluids **10**, 2298 (1998).
[13]C. Wall, B. J. Boersma, and P. Moin, ''An evaluation of the assumed beta probability density function subgrid-scale model for large eddy simulation of nonpremixed, turbulent combustion with heat release,'' Phys. Fluids **12**, 2522 (2000).
[14]H. Pitsch and H. Steiner, ''Large-eddy simulation of a turbulent piloted methane/air diffusion flame (Sandia flame D),'' Phys. Fluids **12**, 2541 (2000).
[15]S. Stolz and N. A. Adams, ''An approximate deconvolution procedure for large-eddy simulation,'' Phys. Fluids **11**, 1699 (1999).
[16]B. J. Geurts, ''Inverse modeling for large-eddy simulation,'' Phys. Fluids **9**, 3585 (1997).
[17]S. B. Pope, *Turbulent Flows* (Cambridge University Press, Cambridge, 2000).
[18]A. A. Townsend, *The Structure of Turbulent Shear Flow* (Cambridge University Press, Cambridge, 1976).
[19]C. Pantano, ''Compressibility effects in turbulent nonpremixed reacting shear flows,'' Ph.D. thesis, University of California, San Diego, 2000.
[20]R. W. Bilger, ''Turbulent flows with nonpremixed reactants,'' in *Turbulent Reacting Flows*, edited by P. A. Libby and F. A. Williams (Springer-Verlag, Berlin, 1980).
[21]F. Higuera and R. Moser, ''Effect of chemical heat release in a temporally evolving mixing layer,'' CTR Report, 1994, pp. 19–40.